5-2017

Computer Simulation of Pore Migration Due to Temperature Gradients in Nuclear Oxide Fuel

Ian Wayne Vance
University of Arkansas, Fayetteville

Computer Simulation of Pore Migration Due to Temperature Gradients in Nuclear Oxide Fuel

A thesis submitted in partial fulfillment
of the requirements for the degree of
Master of Science in Mechanical Engineering

by

Ian Vance
University of Arkansas
Bachelor of Science in Mechanical Engineering, 2014

May 2017
University of Arkansas

This thesis is approved for recommendation to the Graduate Council.

Dr. Paul Millett
Thesis Director

Dr. Arun Nair
Committee Member

Dr. David Huitink
Committee Member

ABSTRACT

A phase-field simulation model is being presented that captures the thermal-gradient-driven migration of pores in oxide fuel associated with fuel restructuring. The model utilizes a Cahn-Hilliard equation supplemented with an advection term to describe the vapor transport of fuel material through the pore interior due to gradients in vapor pressure. In addition, the model also captures changes in a migrating pores' morphology. Simulations demonstrate that the model successfully predicts pore migration towards the hottest portion of the fuel, the centerline. The simulations also demonstrate changes in pore shape that are in agreement with previous experimental observations. Initially isotropic pores are shown to evolve during migration into either a lenticular or a prolate morphology depending on the vapor transport conditions. In addition to the isotropic pores; elliptical initial morphologies are also shown to migrate and experience shape change. This model is the first to simulate the vapor transport mechanism and concurrent changes to a pore's shape during migration. It is a necessary step in performing accurate simulations of the unique and complicated process known as oxide fuel restructuring.

ACKNOWLEDGMENTS

I would first like to thank my major advisor, Dr. Paul Millett. His help and guidance over the last few years have made all of this possible. I am very fortunate to have such a talented and knowledgeable professor. Dr. Millett was always there to provide the tools needed for the completion of this thesis.

I would also like to acknowledge financial support from the Idaho National Laboratory, and all the members of the Nuclear Fuels & Materials and Fuels Modeling and Simulation team. Especially Yongfeng Zhang and Michael Tonks who were always more than willing to answer any questions I had along the way. This research was also supported by the Arkansas High Performance Computing Center, which is funded through multiple National Science Foundation grants, and the Arkansas Economic Development Commission.

Finally, I would like to thank my friends and family. I have always been able to rely on them throughout the years and have depended on their support and encouragement. Thank You.

TABLE OF CONTENTS

LIST OF FIGURES

CHAPTER 1

INTRODUCTION

1.1 Background

Oxide fuels used in reactors are made from ceramic powder, and the process of creating them is not capable of achieving 100% theoretical density. As-fabricated UO_2 fuel pellets contain 5-10% porosity after compaction sintering. Nuclear reactors operate at very high temperatures that cause steep thermal gradients to develop within the UO_2 fuel pellets. The thermal gradients can exceed 1000 K/cm and are capable of driving a unique microstructural change known as pore migration (Olander, 1976). Pore migration refers to the porosity initially present in the fuel and how it migrates radially inwards to the central and hottest portion of the fuel. The migration of the pores results in a large centralized pore that directly affects the fuels performance (MacEwan and Lawson, 1962).

Pore migration results in many microscopic changes that occur during the complicated process of oxide fuel restructuring. The most prevalent is the formation of a central pore. However, it also results in the formation of large inwardly oriented columnar grains in the region immediately surrounding the pore (MacEwan and Lawson, 1962). These columnar grains replace the equiaxed grain structure initially present in the fuel element. The formation of the columnar grains is attributed to the migration of lenticular shaped pores. Lenticular pores are one of two distinct pore shapes that have been observed experimentally. It has been documented that a migrating pore's shape can transform into either a lenticular or a prolate morphology based on the pores initial radial location (Sens, 1972).

The physical driving mechanisms behind pore migration have been debated for years and many theoretical explanations have been considered. However, current research has identified two basic mechanisms to explain the phenomenon. The two mechanisms are solid-state thermodiffusion and vapor transport. Solid-state thermodiffusion, or Soret-effect diffusion (Platten, 2006), is the primary driving mechanism for sub-micron diameter pores and is explained by atomic diffusion along the pore surface or within the solid. The temperature and concentration gradients present in the fuel act as driving forces for solid-state diffusion. Vapor transport, or the evaporation-condensation mechanism, deals with relatively large pores (>1 μm) and is explained by the diffusion of the solid material across the inside of the pore. The driving force for the vapor transport mechanism is the variation of the vapor pressure of the solid material with temperature inside the pore (Sens, 1972). This mechanism is characterized by the evaporation of solid fuel material on the hot side of the pore and condensation of said material on the cold side of the pore. Many theoretical treatments of the vapor transport mechanism have been performed, but the models of Nichols (1967,1968,1972) and of Sens (1972) are often the most cited descriptions.

The initial porosity of as-fabricated fuel consists primarily of pores larger than a few microns, and it is the migration of these large pores in their lenticular morphology that most dramatically influences changes to the grain structure (Sens, 1972). Therefore, a computer simulation for the vapor transport mechanism that can capture the changes in pore shape during migration could prove very useful but has yet to be developed. Many models have been produced in the past that use phase-field and Monte Carlo methods to show pore migration in a temperature gradient. However, past models have used a thermodiffusion model to drive pore migration even though theoretical descriptions predict the vapor transport to be dominant.

Furthermore, these models use a constant initially circular pore shape despite experimental observation of non-equilibrium geometries.

1.2 Why Study Pore Migration?

It is well understood that the microstructure of a material is directly related to the performance of said material on the continuum scale. Therefore, it is desirable to fully understand the microstructure of a material in order to achieve the best performance possible. This is certainly the case when dealing with the oxide fuel used in certain nuclear reactors. The microstructure of a UO_2 fuel pellet will change drastically due to pore migration. The primary consequence of pore migration is a non-homogeneous density distribution in the fuel (Sens, 1972). The migration of pores to a central pore will cause a densification of solid fuel at the periphery of the fuel. This will have a direct influence over the distribution of fission power and the thermal conductivity of the fuel. Both factors will affect the temperature distribution, which now varies in time since pore migration itself is not an instantaneous process. The grain structure of the fuel is also altered by the migration of lenticular shaped pores (Nichols, 1979). The initial equiaxed grain distribution is replaced with large columnar grains oriented towards the fuel centerline that will also affect the fuel behavior.

It is necessary to be able to accurately predict the behavior and physical properties of oxide fuel in order to benefit from it the most. This work serves to help understand the mechanisms that lead to the formation of microstructures that characterize pore migration in oxide fuels. Computer simulations that are able to model thermal gradient driven pore migration and its driving forces can provide critical insight. For this reason, pore migration has been studied extensively and some models have been developed that incorporate a solid-state

thermodiffusion model to drive pore migration. These models have been able to produce pore migration in the high-temperature direction but have not been able to reproduce the change in pore shape during migration that experimental research has observed. Thermodiffusion models certainly have their place, but numerous theoretical descriptions predict that the vapor transport mechanism is the dominant controlling mechanism.

Based on the literature, there is a need for a computational model to be developed that describes pore migration due to vapor transport and captures the drastic changes in pore shape during migration for the first time. This thesis serves to develop and present that model.

1.3 Objectives Of The Thesis

The objective of this thesis is to study pore migration and morphology changes in thermal gradients due to the vapor transport mechanism through the use of mesoscale phase-field modeling techniques. A computational model has been built to simulate this type of microstructure evolution using a combined Cahn-Hilliard diffusion-advection equation that uses a widely accepted analytical expression for the transport velocity of gaseous UO_2 as a function of temperature and temperature gradients [see Eq. (25) in Sens (1972)]. The simulations used in this work were developed and performed in the MATLAB environment. The simulations will treat vacancy concentration as a conserved variable and will show that a pore will behave in conjunction with relevant literature by measuring changes in shape morphology and migration velocity. The specific goals of this thesis are as follows:

1. Develop a mesoscale phase-field model that incorporates thermal gradient-driven migration of pores in oxide fuel due to the vapor-transport mechanism. Simulations should show that the model follows the following standards:

- The model developed should predict pore migration toward the centerline of the fuel while demonstrating concurrent changes in pore shape during migration from an initially isotropic morphology.
- Both lenticular and prolate morphologies should be observed in accordance with changes to the supplied transport velocity equation.

2. Develop a parametric study to compare the magnitude of pore migration velocity during simulation to the supplied transport velocity equation. This study is necessary to determine if changes in pore shape influences the velocity of a migrating pore.

1.4 Thesis Organization

This thesis is divided into six (6) chapters. Chapter 1 is an introduction to the type of research performed and provides on overview of the scope of this work. Chapter 2 serves to provide a brief overview of the characteristics of pore migration and the influencing factors. Chapter 3 reviews relevant research work on pore migration including theoretical, computational, and experimental research. Chapter 4 explains how the model in this work was built and the methodology behind the simulations performed. Chapter 5 will present the results of the research performed for this thesis and discuss them appropriately. Chapter 6 is devoted to conclusive remarks and a discussion of possible future works.

CHAPTER 2

PORE MIGRATION CHARACTERISTICS

2.1 Introduction

Pore migration is a type of unique microstructure evolution characteristic of oxide-based nuclear fuels. A general knowledge of this type of evolution is necessary in order to study it using either computational modeling or experimentation. This chapter is presented in order to provide a brief overview of pore migration including why it happens, how it happens, and its consequences.

2.2 Overview

Nuclear reactors operate at high temperatures and an extremely harsh environment is created for the materials, in particular the ceramic oxide-based fuels used. Temperature gradients in the fuel can exceed 1000 K/cm in such reactors. The large thermal gradient caused by the irradiation of the fuel leads to a unique fuel restructuring evolution that happens early in the fuels lifetime, on the scale of hours (Olander, 1976). The fuel contains an initial porosity of 5-10% that is homogenously dispersed throughout the fuel matrix as irregularly shaped pores after compaction sintering. This initial porosity migrates radially inward toward the center of the fuel pellet due to the steep thermal gradient and coalesces into a larger centralized pore (MacEwan and Lawson, 1962).

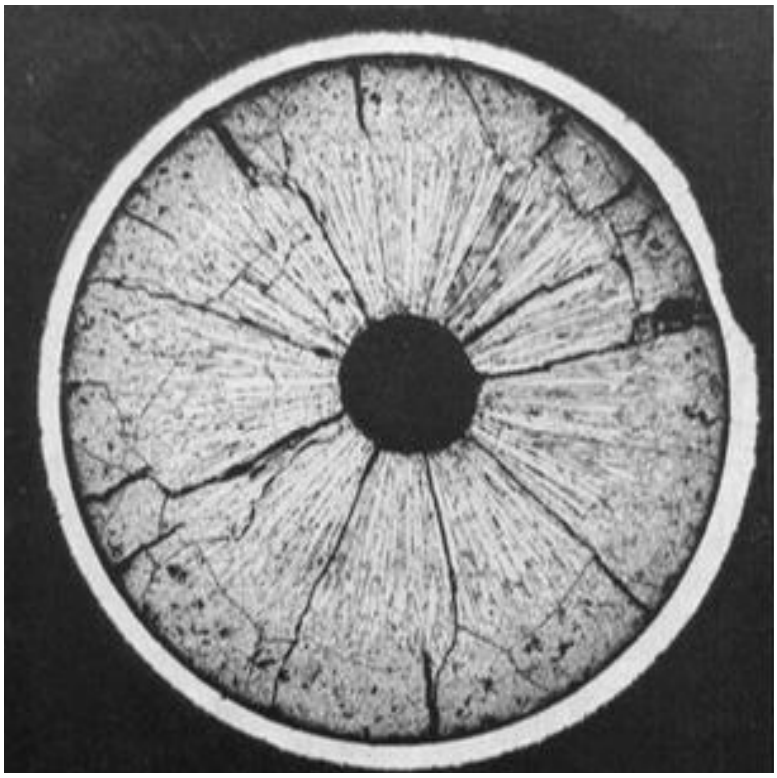

Figure 2.1. Irradiated fuel pin overview
Cross-section of an irradiated fuel pin that shows a central cavity at the center of the fuel element and a collection of columnar grains surrounding the central cavity (Sens, 1972).

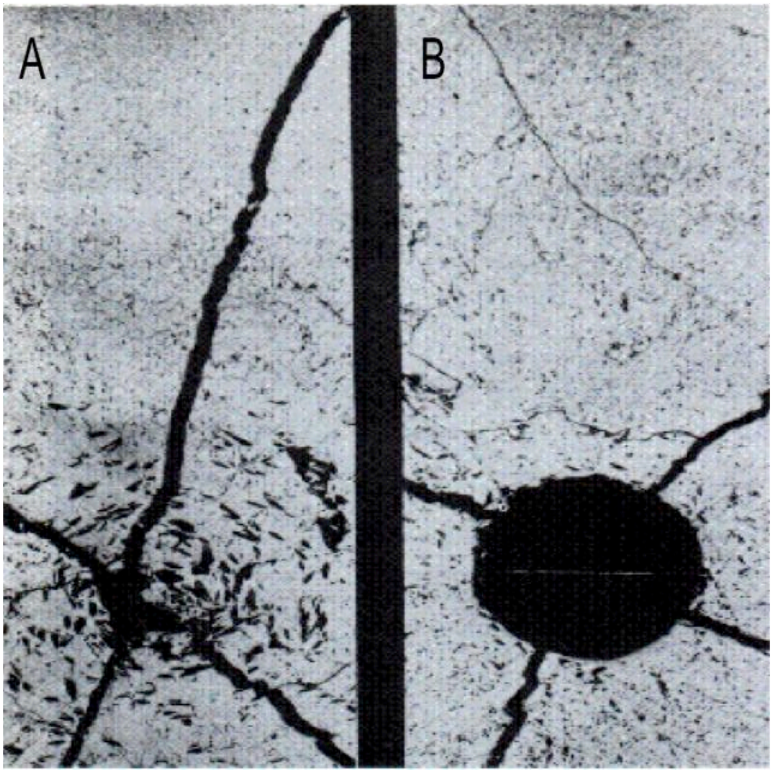

Figure 2.2. Creation of central cavity
The center of an irradiated fuel pin is shown. (A) Lenticular shaped pores migrate and cluster at the center of the fuel pin. (B) The picture on the right, at a later time than section A, shows that a central cavity is formed from the coalescence of the pores shown in part A (Sens, 1972). The dark lines present in figure are cracks in the fuel element.

Migrating pores have been experimentally observed to take on either a lenticular morphology or a prolate (bullet-shaped) morphology depending on their initial radial location and orientation (Sens, 1972). The substantial redistribution of porosity, particularly of the lenticular pores, alters the grain structure of the fuel by replacing the initial equiaxed grain structure with relatively larger columnar grains in the inner one-third of the fuel element (MacEwan and Lawson, 1962). The columnar grains are oriented inwards toward the fuel center. The radially oriented migration path of the porosity follows the direction of the thermal gradient towards the center and hottest portion of the fuel. This process of a mobile phase moving toward a "hot" side is known as the Soret Effect (Platten, 2006) and is based on the

phenomenon of thermophoresis. One consequence is that pores will pick up fission gas during migration and deposit it the central cavity. The means that pore migration serves as a way of removing fission gases and byproducts from the fuel, and depositing them into the central pore.

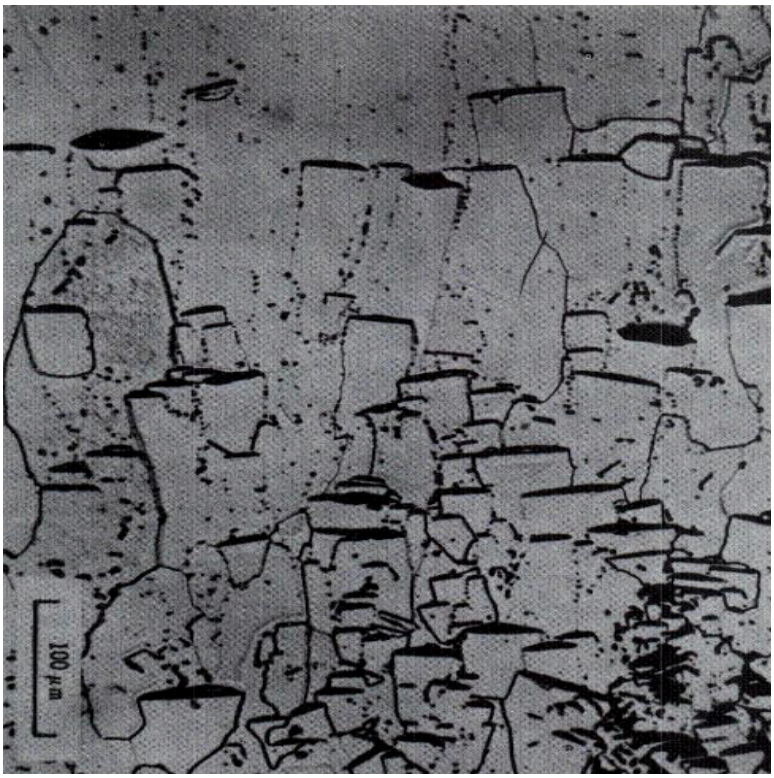

Figure 2.3 Migrating lenticular pores
Lenticular pores are migrating up the temperature gradient in UO_2. Here the temperature increases from the bottom of this figure to the top (MacEwan and Lawson, 1962).

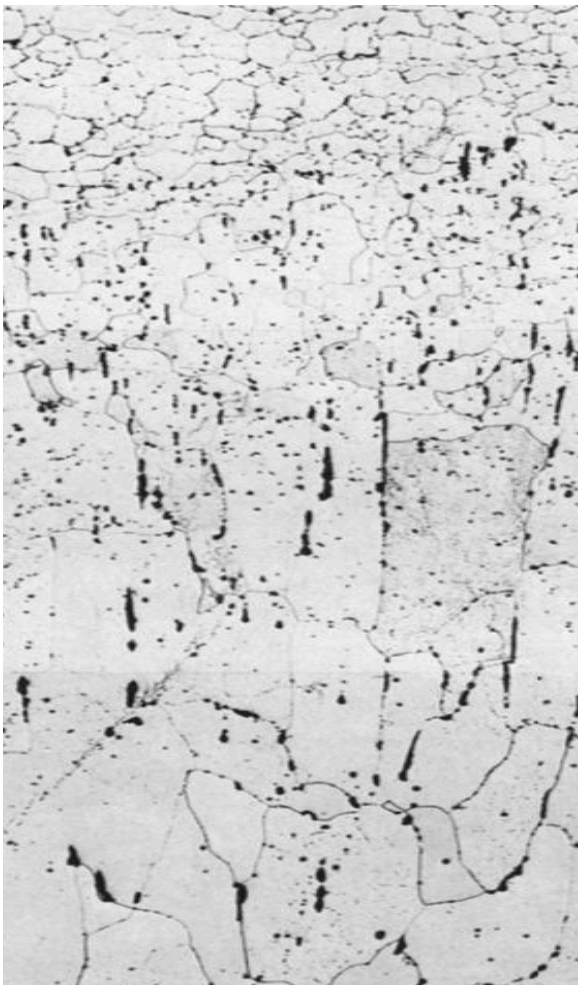

Figure 2.4. Radially oriented prolate shaped pores
Radially oriented pores known as bullet or prolate shaped. The pores are shown along the circumference of the columnar grain region and are pointing towards the center of the fuel (bottom) (Sens, 1972).

Cracks in the fuel element can act as a source of lenticular pores during irradiation and will continue to follow the thermal gradient towards the center of the fuel element (Sens, 1972). These cracks are often created from the thermal stresses on the fuel element but can be repaired by the very pores they emanate. This reparative process could be due to the vapor transport mechanism and how it can produce single-crystal material in its wake (Olander, 1976).

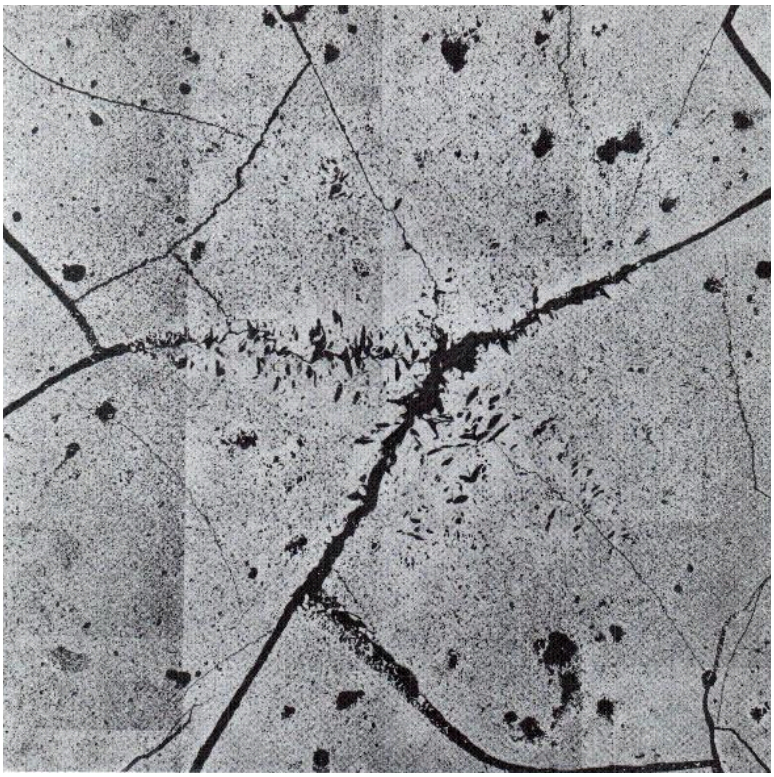

Figure 2.5. Crack acting as a source of lenticular pores
Example of a crack that is acting as a source of lenticular pores (Sens, 1972).

2.2.1 Controlling And Driving Mechanisms

Though the physical origins of thermal gradient pore migration have been considered for years; two basic mechanisms are generally considered when explaining pore migration; the surface-diffusion mechanism and the vapor-transport mechanism. Surface-diffusion uses a temperature gradient as a secondary driving force in addition to the conventional concentration gradient driving force. However, the driving force behind vapor-transport is the variation of the vapor pressure of the solid material with temperature inside the pore. This variation of pressure causes the evaporation of the fuel material (UO_2 molecules) on the hot side of the pore and the likewise condensation of material on the cold side of the pore.

2.2.2 Initial Size Influence

There is no evidence to show that a pore will migrate due to only one mechanism. Speight (1964) developed theoretical models for pore migration for both mechanisms, and showed that the total pore velocity for spherical pores is the sum of both surface diffusion and vapor transport. Speight also found that the two different mechanisms will dominate at different ranges of pore size. Other researchers such as Sens (1972) believe that one mechanism will contribute significantly more to the velocity than the other. Factors exist that limit the influence of each mechanism by adjusting the magnitude of its impact on migration velocity. In practice, the mechanism that produces the highest migration velocity is considered responsible for the motion. According to theoretical derivations, the pore size is understood as the key indicator of which physical mechanism will yield the highest speed and thus be the controlling mechanism. Surface-diffusion is the dominant mechanism of small pores (<1 μm), and conversely, the vapor-transport mechanism dominates pore migration when pore size exceeds just a few microns.

Theoretical derivations show that each mechanism presented dominates the migration velocity at different regimes of pore size (Olander, 1976) (Speight, 1964). Pore velocity due to the solid-state thermodiffusion mechanism is inversely proportional to the diameter of the pore. This inverse relationship has been qualitatively verified by Cornel and Williamson (1964). This relationship leads researchers to believe that this mechanism dominates pore migration at the nanoscale. Contrarily, theory states migration due to vapor transport is independent of pore size and thus the most likely mechanism responsible for the migration of larger pores. As an example, the limiting pore size at 2000 K is 1 μm; meaning that pores with a diameter at or above 1 μm will migrate due to the vapor transport mechanism (Sens, 1972).

2.2.3 Pore Characterization: Location And Shape

The density of nuclear oxide fuels is over 90% theoretical density. A higher fuel density means higher energy output during irradiation, but some porosity is desirable in the as-fabricated fuel in order to accommodate fission-product swelling (Olander, 1976). The remaining pore volume is homogeneously distributed in the fuel matrix as irregular shaped pores. Two primary shapes of pores have been experimentally observed during pore migration, lenticular and prolate. Lenticular shaped pores are oriented with their major axis perpendicular to the direction of temperature gradient and prolate pores are generally found in the outermost region of the fuel with major axis aligned parallel with the temperature gradient. Lenticular pores are generally concentrated in the inner one-third to two-thirds of a fuel pellet while prolate pores are primarily found on the peripheral regions. The characteristic morphologies are a consequence of the transport mechanism that causes migration. The lenticular shape is caused when the trailing edge of the pore is moving at the same speed as the leading edge and midplane of a pore when starting from an initial disc shape. A radially oriented bullet shape is the result of the leading edge moving faster than the rest of the pore when starting from an initial sphere shape (Sens, 1972).

2.2.4 Pore Redistribution And Its Consequences

Nuclear fuel usually consists of cylindrical pellets created from ceramic oxides with a density above 90% where the remaining percentage pertains to pore volume. Pore volume in the fuel pellets, or as-fabricated fuel, is homogenously dispersed as irregular shapes and most have diameters exceeding 1 μm. This type of closed pore is usually filled with a low-pressure gas that is composed primarily of helium, which is used as a cover gas during the fuel-element assembly. This relative large size for pores means that vapor transport is the dominating mechanism for the

majority of porosity redistribution (Sens, 1972). Surface diffusion is primarily responsible for the smaller pores, as discussed earlier, and these small pores are usually created from the precipitation of fission gases during irradiation. The resulting pores usually have a radius less than 0.5 μm and are mainly filled with Xenon at high pressure (Olander, 1976). After a reactor is engaged and the fuel element has been irradiated, it is exposed to a steep temperature gradient that causes the as-fabricated porosity to migrate toward the center and hottest portion of the fuel. The restructured fuel element can be subdivided into a columnar-grain immediately surrounding the central pore, followed by a region of equiaxed grain structure, and finally an area at the periphery known as unstructured because few changes occur due to restructuring. Since the porosity of the fuel is now localized at the centerline of the fuel as a 'central pore', solid fuel is relocated to the periphery. The solid fuel acts as a nuclear heat source and a redistribution of this heat source will result in a temperature profile different than in the as-fabricated fuel. Most notably, the heat source is now located closer to the heat sink and coolant that is surrounding the fuel pellet, and the reduction of temperatures in the inner-most region of the fuel. Not only has the distribution of fission power changed but also the thermal conductivity of the fuel element will vary between areas of large porosity, such as the central pore, and the dense solid fuel in areas with little or no porosity. These effects will result in a change to the temperature distribution. This restructuring means that low-rated fuel rods will theoretically never reach a steady state during their lifetime. However, numerical computations have been performed that couple the temperature distribution and porosity distribution of restructured fuel. These calculations show that the rate of restructuring will decelerate quickly over a few days' time and converge to a quasi-steady-state situation.

CHAPTER 3

LITERATURE REVIEW

3.1 Introduction

The unique microstructure evolution of thermal gradient driven pore migration is a complicated process whose physical origins have been considered for decades with varying degrees of success. The complicated nature of this phenomenon is in no small part due to the numerous variables that influence it. It has been documented through experimental observations that a pore can exhibit a change in shape during migration. It can be rationally concluded that the shape morphology of a pore will have a degree of influence over the fast reactor oxide fuel restructuring process. Therefore, it is beneficial to perform a literature survey in order to understand the current state of relevant research. Relevant research in this breadth has been identified as the mechanisms that have been proposed to explain pore migration and how they have been examined theoretically, computationally, and experimentally.

3.2 Vapor Transport /Evaporation-Condensation Mechanism

The center of the fuel element is its hottest portion with the temperature profile decreasing as the outside edge of the fuel pellet is approached. This means that every pore, regardless or shape or orientation, can be viewed as having a hot side, closest to the center, and a cold side, closest to the outside edge. Large pores can attribute their mobility during the pore migration process to the vapor transport of matrix material from the hot side of the pore to the cold side through the contained gas. The physical driving force behind this mechanism is the variation of the vapor pressure of the solid with temperature, thus resulting in being termed vapor

transport. However, the deposition of material from hot side to cold side means this mechanism is also referred to as the evaporation-condensation mechanism. The models of Nichols (1967,1968,1972) and of Sens (1972) are the most often cited description of the vapor transport mechanism.

The as-fabricated fuel may be a polycrystalline compact, but the matrix material deposited on the cold side of the pore during vapor-transport tends to condense into a nearly single-crystal configuration. Therefore, there exists a grain boundary between the cylindrical columnar-grain region and its surrounding region due to a mismatch of crystal orientations. The peripheral trails of the migrating pores are believed to be in part due to this grain boundary. The grains formed in this way are radially oriented and termed columnar grains due to their resemblance. The trails of migrating lenticular pores can be seen resembling a series of small spheres rather than the straight lines often associated with normal grain boundaries. Sens argues these spheres are simply smaller pores pinched off from the larger parent pore during migration. Conversely, Oldfield and Markworth (1969) argue that impurities are rejected from the migrating pore as small bubbles along the advancing periphery. The latter of which would serve to explain how a migrating pore deals with nonvolatile impurities that would build up on the hot side of the pore and eventually slow down or stop migration if not rejected in some way.

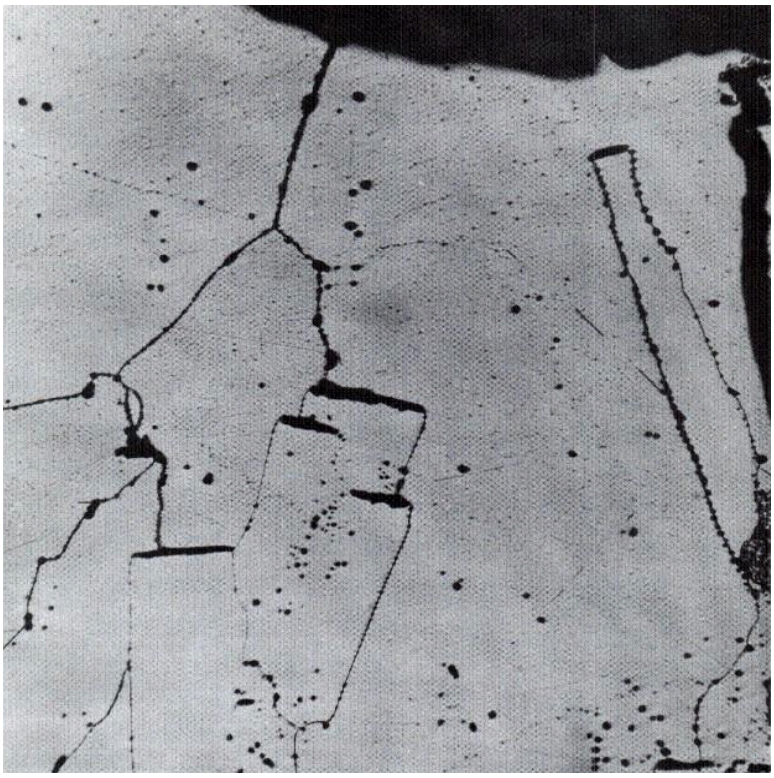

Figure 3.1. Lenticular pores with trailing edges
Lenticular pores are migrating towards the central cavity (top right). Small bubbles can be seen trailing along their periphery (Nichols, 1968).

It has been noted that the migration velocity of typical pores containing low-pressure gas is largest for the vapor-transport mechanism, and therefore focus can be given to this process when considering pore migration (Olander, 1976). This is a result of the as-fabricated fuel containing porosity with average dimensions on the scale of micrometers.

3.2.1 Pore Velocity Considerations

The migration velocity can be either independent of the cavity radius or proportional to the radius depending on the dominant transport mechanism. The independent case is a result of the gas pressure being considered constant. If the velocity is to be proportional to the radius then the gas pressure is taken as balanced by surface-tension forces. A pore that has its internal

pressure equilibrated by the surface tension would result in a spherical pore, but experimental observations show pores with non-spherical morphologies (Sens, 1972). If the pores remained in equilibrium with the surface tension during migration then the pores would be expected to grow as they approached the centerline, which has not been observed. Therefore, it can be assumed that the pressure in the pores is, to some degree, independent of the surface tension; resulting in a pore whose pressure is only determined by temperature and whose volume remains more-or-less constant during migration. This means that pore migration velocity due to the vapor transport mechanism is independent of pore size.

The migration velocity of a pore appears to be dependent on both temperature and the temperature gradient (Sens, 1972). A distribution of pore velocity can be calculated from a given temperature distribution, but the initial temperature distribution will change when the pore begins to move. Therefore, the velocity and temperature distributions should be adjusted during the process in order for a numerical approach to give accurate predictions. Early approaches proved incorrect because of a diffusion coefficient being too high (Kaneko et al., 1969). The original velocity calculation for vapor transport was given by De Halas and Horn (1963), but other researchers such as Speight (1964), Nichols (1967), and Sens (1972) have improved upon their research by using different considerations and assumptions. For example, Speight (1964) deduced an equation for velocity due to vapor transport that was linearly dependent on pore size, Eq. (3.1), and is based on his derivation of the diffusion coefficient. Speight assumes that the gas bubbles are in equilibrium and therefore created an equation for the internal pore pressure, Eq. (3.2), where γ is the surface tension of the UO_2 fuel, P is the partial pressure of the gas filling the pore, and p is the vapor pressure of the diffusing species.

$$v_v = Ar\frac{dT}{dx} \tag{3.1}$$

$$P + p = \frac{2\gamma}{r} \tag{3.2}$$

3.2.2 Deduction Of The Diffusion Equation

The vapor transport mechanism has the temperature gradient and resulting concentration gradient as driving forces, and both forces must be taken into account in order to accurately represent the mechanism. Analytical models are derived from basic principles and the theory of irreversible thermodynamics. Even with this theory considered, some assumptions must be made. Sens (1972) derived a diffusion equation and a migration velocity equation for the vapor transport mechanism that was used in this research. Sens' assumption for his deductions included:

- vapor transport is the controlling mechanism,
- pores are filled with helium, one atmosphere at room temperature, behaving as an ideal gas,
- UO_2 vapor behaves as an ideal gas, and
- velocity is independent of pore size.

Sens starts by describing the transport of material and of energy from an arbitrary point in the pore given by steady state thermodynamics (Denbigh, 1950).

$$j_E = -L_{11}\nabla(\ln T) - L_{12}T\nabla(\frac{\mu}{T}) \tag{3.3}$$

$$j_i = -L_{21}\nabla(\ln T) - L_{22}T\nabla(\frac{\mu}{T}) \tag{3.4}$$

where

$j_E = energy\ flow, cal/cm^2 * sec$

$j_i = material\ flow, moles/cm^2 * sec$

$L_{ij} = phenomenological\ (Onsager, 1931)\ coefficients\ with\ L_{ij} = L_{ji}$

$\mu = thermodynamic\ potential\ per\ mole$

$T = temperature.$

If the material and energy transport are under isothermal conditions, then the coefficients $L_{12} = L_{21}$ can be expressed in terms of L_{22}, and then $\nabla(\ln T) = 0$.

$$\left(\frac{j_E}{j_i}\right)_{T=constant} = \frac{L_{12}}{L_{i2}} = \frac{L_{21}}{L_{22}} = q \tag{3.5}$$

Where q is defined as the energy per diffusing mole transported in the absence of a temperature gradient. This step allows the equation for the material flow to be rewritten as:

$$j_i = -L_{22}\left\{q\nabla(\ln T) + T\nabla\left(\frac{\mu}{T}\right)\right\} \tag{3.6}$$

The next step involves substituting the Gibbs free energy thermodynamic relations into Eq. (3.6). This is possible because Gibbs energy is a thermodynamic potential used when a system is at a constant temperature and pressure.

$$\mu = u - Ts + pv = h - Ts$$

$$d\mu = -sdT + vdp$$

$$j_i = -L_{22}\left(\frac{q-h}{T}\nabla T + v\nabla p\right) \tag{3.7}$$

Since isothermal conditions are being considered, then Eq. (3.7) must be representative of Fick's first diffusion law. Fick's first law relates the diffusive flux with the concentration under a steady state assumption. It states that the flux will move from regions of high concentration to regions of low concentration with a magnitude proportional to the concentration gradient. Stating isothermal conditions and knowing that Fick's first law is represented by Eq. (3.7), it then becomes

$$(j_i)_{T=constant} = -L_{22}(v\nabla p) = -L_{22}\mathrm{vRT}\nabla\mathrm{c} \tag{3.8}$$

$$(j_i)_{T=constant} = -\mathrm{D}\nabla\mathrm{c} \tag{3.9}$$

where $c = p/\mathrm{RT}$ and is the concentration of the diffusing species. The coefficient, L_{22}, can be solved for by setting Eq. (3.8) and Eq. (3.9) equal to each other. This newly found coefficient could then be substituted back into Eq. (3.7) to achieve:

$$j_i = -\frac{D}{vRT}\left(\frac{q-h}{T}\nabla T + v\nabla p\right) \tag{3.10}$$

The quantity *q*-*h* is defined as the excess energy of the diffusing molecules as compared to the enthalpy of the bulk gas. Nichols (1969) states that the molecules in transit are indistinguishable from the bulk gas and therefore *q* and *h* are equal, resulting in the aforementioned quantity being zero. However, Sens says that Nichols statement is incorrect because the molecules in transit are distinguishable. Sens then derives values for *q* and *h* based on the average translational energy of all molecules in a Maxwell-Boltzmann distribution to show how *q* and *h* are equal and that the quantity is zero. He also states that this result is only valid in a special case of gaseous diffusion when there are no restrictions to the gas stream. Eq. (3.10) then becomes:

$$j_i = -\frac{D\nabla p}{RT} \qquad moles/cm^2 * sec \tag{3.11}$$

Eq. (3.11) describes the flow of UO_2 moles as a function of the temperature and pressure gradients at each point in the pore. Steady state conditions can then be applied to Eq. (3.11) to give:

$$\nabla \cdot \left(\frac{D}{RT}\nabla p\right) = 0 \tag{3.12}$$

The diffusion coefficient used here is given by kinetic gas theory and is stated by Sens (see Eq. (15) in (Sens, 1972)) (Dushman, 1958). Nichols has solved Eq. (3.12) algebraically for an initially spherical pore and claims his equation is correct to second order terms and predicts a change in shape from spherical to lenticular (Nichols, 1968). However, he also predicts that lenticular pores must arise from pores that are initially partially lenticular. Previous work assumed the temperature distribution in the pore is unidirectional, similar to the surrounding fuel

matrix (De Halas and Horn, 1963)(Nichols, 1967). It can then be decided that cross-sectional planes in the pore, that are perpendicular to the direction of the temperature gradient, are isothermal planes in the pore. The vapor pressure on these isothermal planes is determined by the solid-vapor equilibrium at the edge of the planes, along the pore surface, and is given by:

$$\mathrm{p} = p_0 exp(-\Delta H/RT) \tag{3.13}$$

Sens (1972) derives values for p_0 and ΔH from supplied vapor pressure data on UO_2 (Ohse, 1964). Sens also assumes that the cross sectional planes are isobaric in addition to being isothermal and the resulting pressure gradient is unidirectional. This assumption means that the pores will preserve their shape during migration. In order to capture changes to the pores shape during migration then Eq. (3.13) must be restricted to the pore surface where actual solid-vapor equilibrium exists. In order to find the pressure distribution throughout the pore volume, it must be determined as a solution of Eq. (3.12). Sens uses Eq. (3.13) to convert a given temperature distribution along the pore surface into a vapor pressure distribution which is then used as the boundary condition for Eq. (3.12). Once the UO_2 vapor pressure distribution is found then the material flow can be calculated via Eq. (3.11). The molar flow is expressed as the amount of material transported in terms of solid UO_2 of the density at the appropriate temperature. This means a transport velocity is given by:

$$v = -j_i \mathrm{N}\Omega_T = -j_i \frac{M_{UO2}}{\varrho T} \ \ cm/sec \tag{3.14}$$

where

$N = Avogadro's\ number$

$M_{UO2} = molar\ weight\ of\ UO_2$

$\varrho T = theoretical\ density\ of\ UO_2\ at\ temperature\ T$

$\Omega_T = molecular\ volume\ of\ UO_2\ at\ temperature\ T$

$T = temperature$

This velocity is primarily significant at the pore surface because it gives the evaporation and condensation rates. Eq. (3.14) could describe the material transport in the pore as an equivalent velocity.

3.2.3 Migration Velocity Equation

Calculating values for Eq. (3.14) at three key points along a pores surface can be used to describe the motion of the pore. A lenticular or disc shaped pore at steady-state has a transport velocity at the midplane of the pore that is equal to both the leading and trailing edge. Therefore, one of these velocities can be taken to represent the pore as a whole. It is worth restating that concentrating on lenticular pores migrating due to the vapor transport mechanism is justified when considering the microstructural changes in UO_2 fuel rods. Sens arrives at an expression for the transport velocity of gaseous UO_2 as a function of temperature and temperature gradient by combining many of the previously mentioned equations with measured and published material data (see Eq. (25) in (Sens, 1972)).

$$\boldsymbol{\nu} = A(B + CT + DT^2 + ET^3)T^{-5/2}\Delta H\, p_o \exp\left(-\frac{\Delta H}{RT}\right)\left(\frac{dT}{dr}\right)_{matrix}, \qquad (3.15)$$

Variables from Eq. (3.15) are given as: T is temperature, ΔH is the enthalpy of vaporization of UO_2, p_o is a pressure prefactor, and $A - E$ are empirical constants. Sens supplies values for $A - E$, ΔH, and p_o, which allow the transport velocity to be plotted against the fuel radial distance. This equation lets the migration rate of a lenticular pore be calculated for each value of the temperature and the temperature gradient. Thus, with a given temperature distribution in a fuel rod, the pore migration rates as a function of fuel radius can be calculated.

3.3 Surface Diffusion

The surface diffusion mechanism in nuclear fuels refers to the movement of small pores that move both randomly and under the influence of a driving force, but for a pore in a temperature gradient, the temperature gradient causes the diffusion of atoms along the pores' inside surface in a preferential direction, i.e. from the hot region to the cold region. The directional flow of atoms in this prescribed way means the pore will travel towards the hot region of the fuel element, which is in agreement with the vapor transport mechanism described earlier. Differences between the two mechanisms are due to three primary categories; magnitude of predicted velocity, pore size relationship, and the actual mechanism of migration.

Surface diffusion is being driven by a temperature gradient in addition to the conventional concentration gradient, which means that it is a thermodiffusion process. It has also been called surface thermal self-diffusion and Soret-effect diffusion. The Soret-effect is a phenomenon observed in mixtures where the particles of two or more materials behave in different ways in response to an applied temperature gradient. A flux of one species is generated by a temperature gradient and will result in a concentration gradient under steady-state conditions. In the case of surface diffusion, the diffusing species will travel from the hot region to the cold region. It should also be noted that the Soret effect is proportional to the temperature gradient as well (Platten, 2006).

It has already been stated that surface diffusion is the dominating mechanism for pores of small size, usually sub-micron diameters. This is because the migration velocity for surface diffusion is inversely proportional to the pore radius; meaning, the larger a pore is then the less influence surface diffusion will have on its migration velocity. Olander (1976) developed an

equation for the migration velocity of pores due to surface diffusion that is accepted and used in other papers (Desai et al., 2010).

$$\boldsymbol{v} = \frac{3D_S Q_S^* a_0}{kT^2 R}\left(\frac{dT}{dx}\right) \tag{3.16}$$

The variable $\boldsymbol{v}$ is the pore migration velocity, D_s is the surface diffusivity, Q_S^* is the value of the heat of transport for surface thermal self-diffusion, R is the radius of the pore and dT/dx is the temperature gradient. The temperature, T, is taken as the average temperature over the region in which the pore moves. Q_S^* is not readily available and is difficult to calculate, so it is approximated as the activation energy required for surface diffusion (Olander, 1976). D_s and Q_S^* must be calculated for all of the species being considered, uranium and oxygen in the case of nuclear oxide fuel.

3.4 Computational Research

It is exceedingly difficult to observe pore migration with in-situ techniques. Nuclear fuel can be an unforgiving medium for experimental studies due to the large temperatures and other variables that are necessary to accurately represent realistic conditions. Therefore, computational methods provide much needed insight into the subject. Mesoscale simulations are well suited for examining the microstructure evolution of pore migration. Phase field techniques have been shown to demonstrate multiple mechanisms of pore migrations, Monte Carlo methods are well suited for simulating the grain growth evolutions associated with pore migration, and molecular dynamic methods are inherently appropriate for studying pore migration at the atomic scale.

The results of computer simulations in the past have been useful but have not been entirely inclusive. The simulations often result in the migration of pores with velocity in

agreement with analytical models, and the migration is shown in the high-temperature direction, which follows the Soret Effect. However, computer simulations have yet to capture the shape evolution of a pore during migration that has been experimentally observed. This change in shape is usually ignored by most existing theoretical models in favor of a constant shape assumption in order to simplify the problem. There also has not been a mesoscale simulation model that describes pore migration due to the vapor transport mechanism. Capturing migration to the high temperature domain due to the vapor transport mechanism and demonstrating concurrent changes in the pore shape has not been previously achieved.

3.4.1 Phase Field

Phase field methods are well equipped to handle pore migration because they have successfully been used to model and predict the mesoscale morphological and microstructure evolution in materials (Chen, 2002). Additionally, the benefits of phase field techniques did not emerge until around the turn of the century. Thus, most of the research of pore migration in terms of phase field models is all relatively recent and benefits from the decades of research performed by others.

Phase field methods describe a microstructure by using a set of conserved and nonconserved field variables that are determined by the Cahn-Hilliard (Cahn and Hilliard, 1958) and Allen-Cahn (Allen and Cahn, 1979) equations, respectfully. Phase field models used to study pore migration in a temperature gradient have been developed in the past. However, they assumed a thermodiffusion model in order to drive pore migration, which directly contradicts the theoretical models that predict the vapor transport mechanism to be dominant. There are two primary ways in which this has been done; a temperature-dependent free energy function (Hu

and Henager, 2010)(Li et al., 2010) or a flux term containing the temperature gradient (Zhang et al., 2012).

Hu and Henager developed a model in 2010 that was used to study pore migration by both bulk and surface diffusion in a temperature gradient (Hu and Henager, 2010). Their model demonstrated that the migration velocity varied inversely with the pore size and that agrees with the theory for surface diffusion driven migration. This model also showed that the pores migrate up the temperature gradient, which also agrees with theoretical and experimental observations. The intent of this work is to study the effect of temperature gradients and vacancy surface mobility on pore migration. They state that bulk and surface diffusion and the evaporation/condensation of atoms are expected to take place simultaneously during migration. However, the evaporation/condensation mechanism is not included in the model. This paper used a temperature dependent free energy function in order to have the equilibrium vacancy concentration in the matrix and the free energy of the matrix phase decrease with decreasing temperature while having the free energy of the pore phase be independent of temperature (Hu and Henager, 2010). This means that the Soret effect is implicitly contained in the model because a concentration gradient will exist when a temperature gradient exists. The model presented in this paper stands out from others because it is very robust. The model was developed in a way that allows for the impact of vacancy concentration, multi-pore interactions, and temperature gradients on pore migration to be studied.

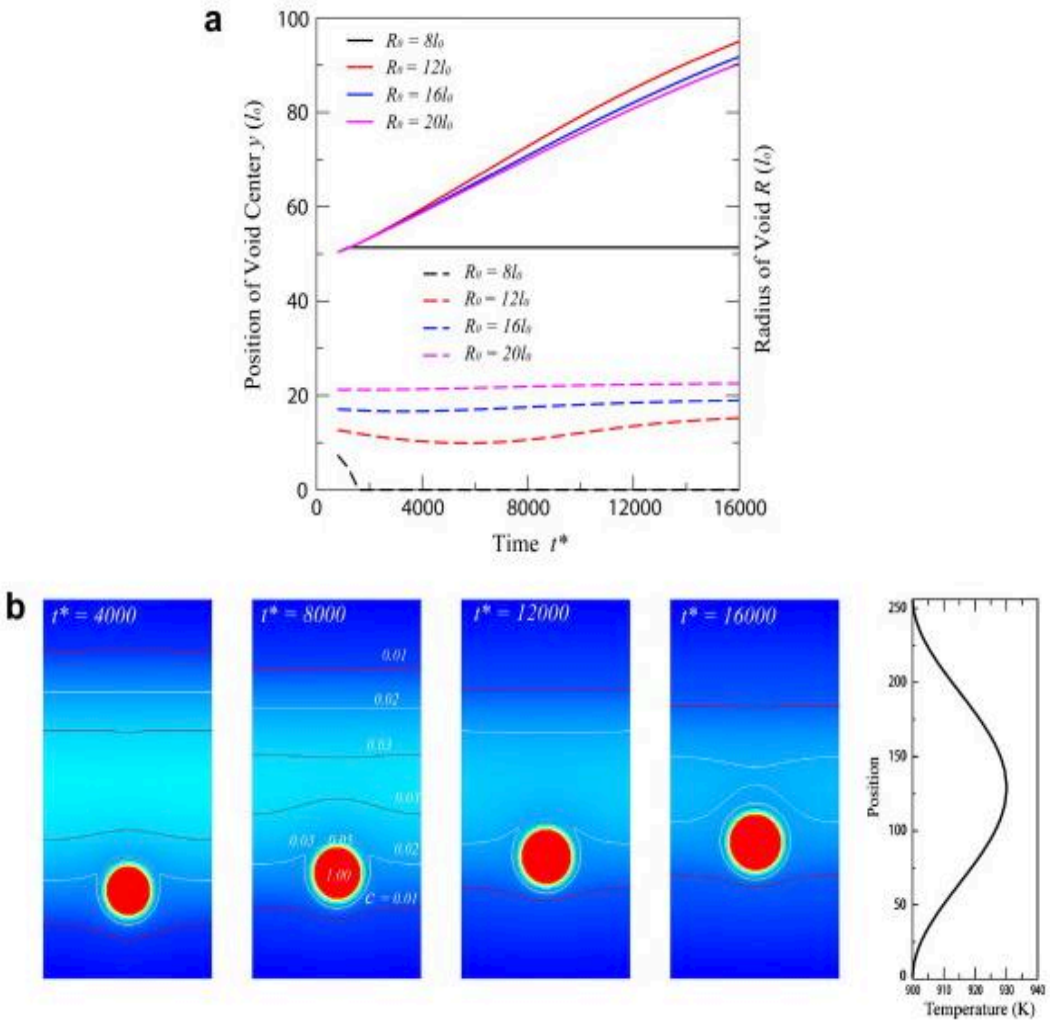

Figure 3.2. Simulation results from Hu and Henager (2010)
(a) Evolution of pore position. The solid lines represent the position of the center of the pore as a function of time and the dashed lines represents how the pore radius changes with time. Multiple radii are shown, $R_0 = 8l_0$, $12l_0$, $16l_0$, and $20l_0$ where l_0=2nm (b) Simulation results for the morphology change of a pore with $R_0 = 16l_0$. A temperature profile is shown on the right side of the figure and is used to show that the pore moves towards the high temperature domain during migration. The pictures in (b) are placed from left to right, beginning to end respectfully. The figure is used to demonstrate the simulation results for the case of M_1=0 (Hu and Henager, 2010).

Hu and Heneger were part of another research paper that was presented shortly after the one previously described, (Hu and Henager, 2010). A team from Pacific Northwest National Laboratory developed a phase field model to study the effects of temperature gradients, vacancy

concentrations, vacancy generation rates, and the recombination of vacancies and interstitials on pore migration and pore growth (Li et al., 2010). This model is similar to what others have presented, namely Hu and Henager, but this paper aims to address the effect of radiation on pore migration and growth kinetics. It extends the work of Hu and Henager (2010) to accomplish the aforementioned goals by assuming bulk diffusion controlled migration, and considering only single vacancies and single interstitials for simplicity. The model demonstrated pore migration towards the high-temperature domain by implanting the Soret effect in the same way as Hu and Henager (2010). The pore migration mobility is found to be independent of pore size, which is in theoretically agreement for bulk diffusion controlled migration. The drawback to this research is that bulk diffusion is no longer considered a primary mechanism for pore migration. The research was successful in concluding that the pore migration mobility is dependent on the temperature gradient and the temperature gradient itself causes vacancies, interstitials, and pores to flow toward the high temperature domain. The researchers postulate that this results in the formation of a central hole, which has been observed in spent nuclear fuel. It is also stated that a thermodynamic database is needed in order for the accuracy of this, and other mesoscale and macro-scale simulations, to be sufficient. This is because the uncertainty of the simulation is dependent on the thermodynamic and kinetic properties used to build it.

The Fuels Modeling and Simulation Department of Idaho National Laboratory published a paper in early 2012 that aimed to simulate temperature gradient driven pore migration coupled with thermal conduction with a phase field model (Zhang et al., 2010). This paper identified a missing component of previously performed research; quantification of the impact of the low thermal conductivity of pores. Theory states that pores will migrate toward the high temperature domain as a result of a temperature gradient driving force. Previous studies often assume a

constant temperature gradient across the fuel element, but the pores will often contain gases that have a thermal conductivity much lower than the surrounding fuel matrix. The low thermal conductivity of the pore will result in an increase of the temperature gradient across the pore. This paper is different from the previous two because here a flux term containing the temperature gradient is introduced in order to represent the Soret effect associated with pore migration. However, bulk and surface diffusion are still considered as the primary mechanisms. The phase field model is implemented with the Cahn-Hilliard format and the heat conduction equation is solved simultaneously to describe the temperature field. In order to study the influence of thermal conductivity, the conductivity is varied spatially based on the different phases of the system. The different phases being calculated from the conserved order parameters of the Cahn-Hilliard equation. The simulations preformed in this paper were successful in demonstrating pore migration toward the hot region of the simulation environment, the model was also validated by comparing displacements with analytical solutions, and it demonstrated the impact of a pores thermal conductivity on the thermal gradient and temperature profile. The paper only considered pore migration in a single crystal and thus did not deal with the influences of grain boundaries and it also did not deal with change in the pores shape.

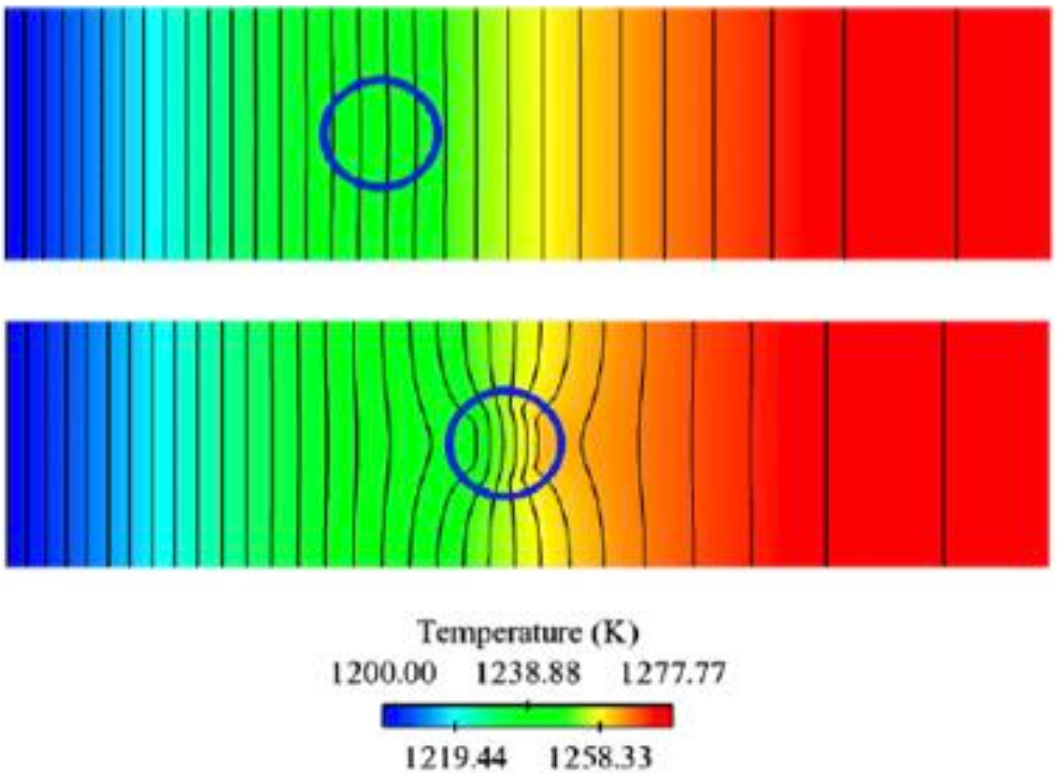

Figure 3.3. Simulation results from Zhang et al. (2012)
Two simulations showing pore migration in a thermal gradient. The top figure is a reference case, and the bottom figure includes thermal conductivity coupling when the pore contains Xe gas. The two figures are shown at the same time step so the difference in position can be observed. The thermal gradient increases inside of the pore in the bottom figure, which is demonstrated by the black marking lines bending towards the center of the pore (Zhang et al., 2012).

Previous phase field simulations show pore migration in the direction of the temperature gradient and often use bulk and surface diffusion as the driving forces behind migration. However, simulations failed to show changes to the shape of pores during the course of migration. This lack of shape change is in disagreement with experimental observations that document highly non-equilibrium geometries. Also, a simulation model has yet to be developed that can describe pore migration due to the vapor transport mechanism.

3.4.2 Monte Carlo

Phase field simulations make up the majority of the computational research that has been done concerning pore migration. However, Monte Carlo techniques have also been used to simultaneously show grain growth, pore migration, and thermal segregation of pores in a thermal gradient (Tikare and Holm, 1998). Tikare and Holm (1998) used a statistical-mechanical Potts Monte Carlo technique in 1998 to model the grain growth kinetics while incorporating conserved dynamics to model pore migration via surface diffusion. Conserved dynamics are used so that the total number of pore sites and grain sites remain constant though the entire simulation. The volume fractions of both grains and pores were assumed constant during the simulation and the model ignored any vacancies that would realistically exist in the matrix.

The standard Metropolis algorithm is used to perform the pore migration step and the grain growth step by determining the transition probability with Eq. (3.17), and where the equation of state is the sum of all the neighbor interaction energies given by Eq. (3.18). Multiple simulation techniques were investigated during this research and they include same spin assignment, random spin assignment, and minimum-energy spin assignment. Tikare and Holm chose minimum-energy spin assignment as the best representation of pore migration through surface diffusion.

$$P = \begin{cases} exp\left(\frac{-\Delta E}{k_B T}\right) & for\ \Delta E > 0 \\ 1 & for\ \Delta E \leq 0 \end{cases} \tag{3.17}$$

$$E = \frac{1}{2}\sum_{i=1}^{N}\sum_{j=1}^{6}\left[1 - \delta(q_i, q_j)\right] \tag{3.18}$$

They introduced a temperature gradient via the interfacial mobility gradient and added a heat of migration term in order to show thermal segregation of the pores and UO_2. This heat of migration term also biased the motion of the pores towards the high-temperature region

demonstrating the Soret Effect. The research was successful in terms of its own stated motivations (Tikare and Holm, 1998), to simulate grain growth and pore migration simultaneously. This method even showed differences in the shape of the pores during migration; however, the change in pore shape is based on the shape of the surrounding grain boundaries and does not resemble any of the commonly observed morphologies typical of oxide fuels. Grain growth was found to be pinned by the pores at the finite Monte Carlo temperature simulated. A notable assumption in this paper is that grain growth and pore migration as well as their driving forces remain constant with temperature. The only variables that are changed are their respective mobility terms.

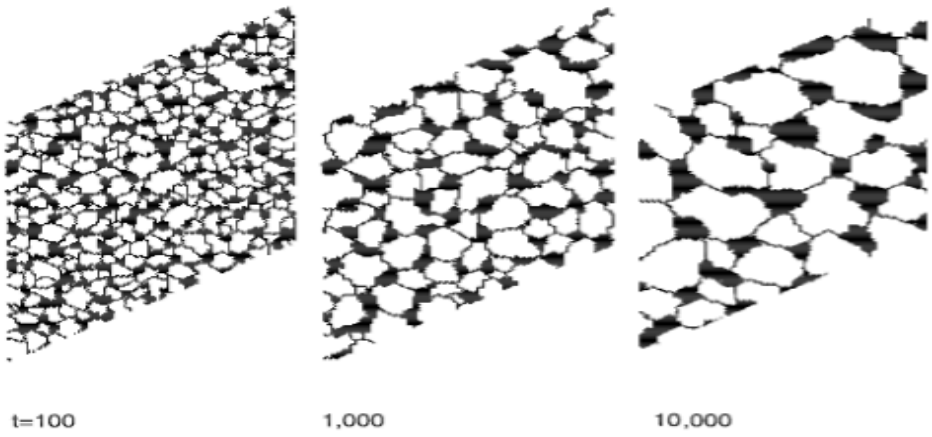

Figure 3.4. Simulation results in an isothermal region from Tikare and Holm (1998)
A Monte-Carlo simulation demonstrates the microstructural evolution from grain growth and pore migration. The simulation shown is for the case of an isothermal region using the minimum-energy spin assignment for pore migration (Tikare and Holm, 1998).

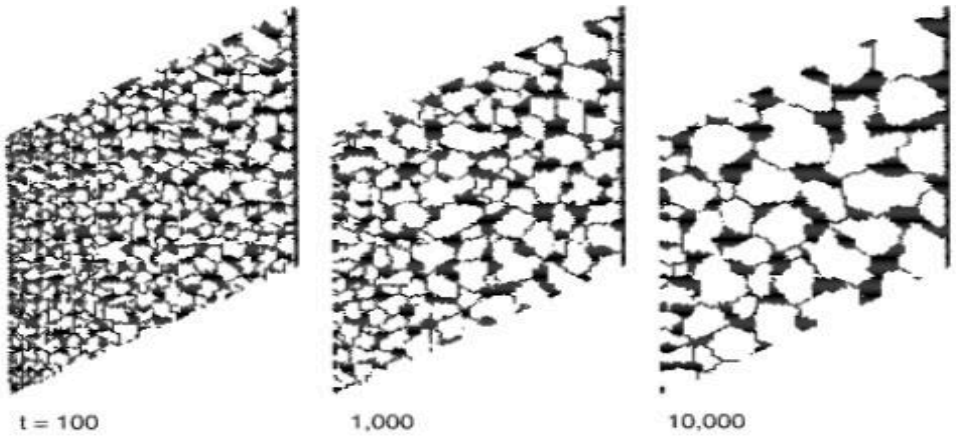

Figure 3.5. Simulation results in a thermal gradient from Tikare and Holm (1998)
Results from a Monte-Carlo simulation that shows microstructural evolution from grain growth and pore migration. The simulation is for the case of a thermal gradient being present, and demonstrates a higher grain growth rate and larger pores compared to Figure 3.4. The left side of the simulation domain corresponds to the cold side and the hot region corresponds to the right side (Tikare and Holm, 1998).

3.4.3 Molecular Dynamics

As stated earlier by analytical and theoretical models, surface diffusion is the primary mechanism responsible for pore migration at the submicron scale. Therefore, the phase field and Monte Carlo methods previously discussed are not optimal for simulating the atomic processes that control the migration of nanometer sized pores. Molecular dynamics is a technique that allows the simulation of individual atoms and their interactions and is thus a great method for simulating surface diffusion. A paper, 2010, from Desai, Millett, Tonks, and Wolf at Idaho National Lab performed atomistic simulations of nanometer sized pores which serves to understand the atomic processes involved in migration (Desai et al., 2010).

Molecular dynamics simulations were performed on single crystal UO_2 with pores of 2.2 nm with an external temperature gradient applied across the simulation cell. The simulations showed migration of the pore towards the high-temperature domain and captured data for the migration velocity of the pores. The velocities were then compared with available

phenomenological equations for pore migration due to different transport mechanisms. The mechanism with values most closely matching the data from the simulations was determined to be the dominant mechanism for pore migration. The dominant mechanism in this case was found to be surface diffusion of the slowest moving species, i.e. uranium. This paper also found that other contributions from lattice diffusion and the thermal stress gradient, which is due to the applied temperature gradient, were negligible. This type of simulation and its post processing also serves as a method of identifying the point at which the dominant mechanism crosses over from diffusion-controlled mechanisms to a lattice-diffusion-controlled mechanism. This crossover point was found to be for pores in the micron range, which is in agreement with past papers.

The simulations performed in this paper demonstrated pore size and shape that remained stable and constant during the migration process. Since this paper compares data with phenomenological equations, which contain a basic assumption of constant pore shape, then constant shape must be assumed here as well. Lattice diffusion can be presumed to be non-dominant because no lattice diffusion was observed for ions away from the pore. Furthermore, the paper also presents a figure in which a single atom, represented by a black color, is monitored for multiple time steps. The single atom is initially shown to lie in the high temperature region of the pores surface and then moves along the pores surface towards the cold temperature region as the simulation progresses. This ability to follow a single atom demonstrates evidence for researchers to presume surface diffusion.

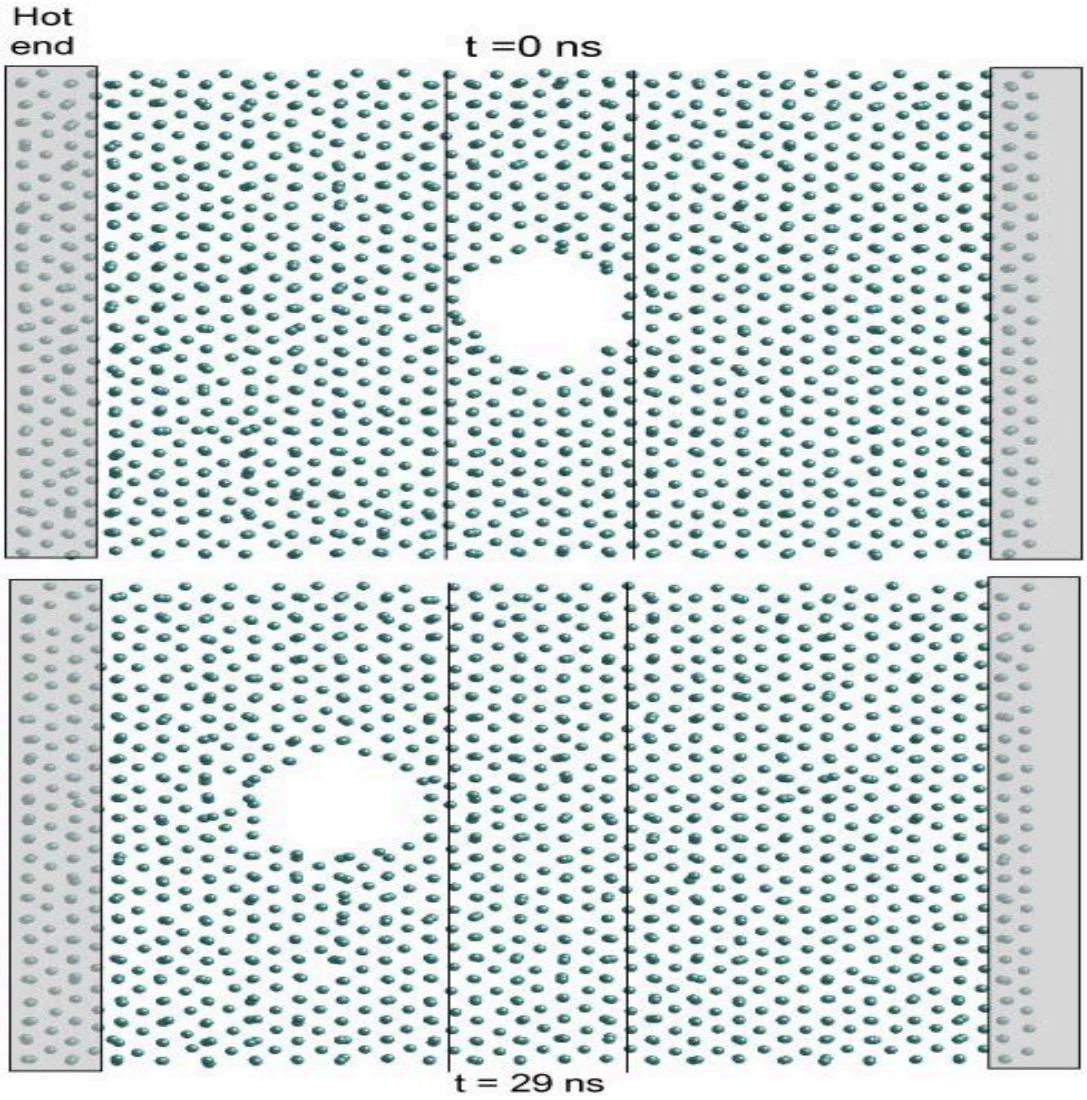

Figure 3.6. Simulation results from Desai et al. (2010)
Snapshots taken at 0 and 29 ns during an atomistic simulation performed by Desai et al. (2010). The snapshots demonstrate pore migration toward the hot side of the simulation cell, which corresponds to the left side of the figure. Two black lines are placed at the center to act as guidelines for the eye.

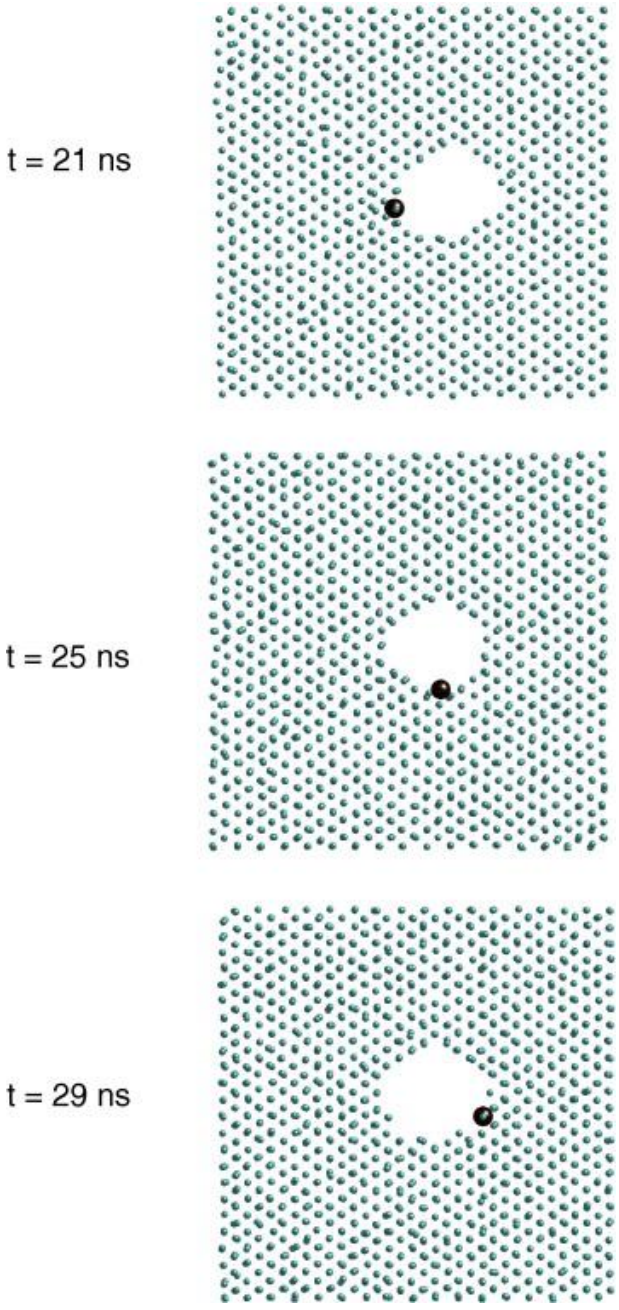

Figure 3.7. Single atom tracking from Desai et al. (2010)
Atomistic simulation highlighting a single atom. Snapshots are taken at 21, 25, and 29 ns and are shown from top to bottom respectfully. A single atom is enlarged and is shown in a different color from the other atoms. The purpose of this is to be able better visualize the bath of diffusion that is taking place during migration. The atom can be seen staring near the hot side of the simulation cell and moving along the surface towards the cold side of the domain. Multiple atoms following similar paths of diffusion would result in a pore migrating towards the hot side (Desai et al., 2010).

3.5 Experimental Research

MacEwan and Lawson (1962) performed an early experimental study in 1962. This particular experiment focused on inducing columnar grains to grow in high-density sintered uranium dioxide specimens. They achieved this by introducing a steep temperature gradient into the specimen, but were careful to remain below the melting point. Though this experiment was not focused on pore migration, it was able to demonstrate that a temperature gradient high enough to cause columnar grains could be introduced without melting the specimen. Columnar grains are known to develop from the migration of lenticular pores and thus the methodology of this experiment could be expanded for further studies into pore migration.

Michels, Poppel, and Niewmark in 1970 measured migration velocities of gas bubbles and solid inclusions while comparing their results with equations for surface thermal self-diffusion (Michels et al., 1970). The pores ranged from 1 to 5 μm and their findings were between 2 and 5 times higher than the velocities predicted by Eq. (3.16). They also did not observe any noticeable relationship between velocities and pore radius which is contrary to surface diffusion theory (Michels et al., 1970). However, their findings at this time provide some evidence that surface diffusion may not be the controlling mechanism for large bubbles. The experiments also noted that the solid inclusions migrated up the temperature gradient but with velocities that decrease as the size of the inclusion increased which matches the surface diffusion relationship. Surface diffusion for inclusions makes sense because the inside of a given cavity is occupied and the vapor transport mechanism will not be able to occur.

The Power Reactor and Nuclear Fuel Development Corporation released a paper in 1977 in which researchers attempted to measure the migration rates of lenticular pores and compare their results with the theoretical values derived from Sens' model and Nichols's model

(Kawamata et al., 1977). Lenticular pores are chosen as the focus of this paper because, as they state, the lenticular pore is most commonly observed in irradiated fuel and is responsible for the formation of columnar grains due to their migration by the vapor transport mechanism (Kawamata et al., 1977). Disc shaped pores were fabricated in the interface of two thin discs of UO_2 using a resintering process. The pores were then allowed to move under the influence of a temperature gradient via an induction furnace, and their migration rates were measured. The migration distances can be measured after the experiment and will lead to the migration rate when divided by the heating time. The temperature gradient was found by dividing the temperature difference of the two sides of the specimen by its width. The paper concludes that the observed migration rates are in good agreement with Sens' model. Although "good" is a relative term that could be argued, Sens' model certainly matches better than that of Nichols and leads to a conclusion that the temperature gradient in the lenticular pore is approximately four times as large as the fuel matrix. It should also be noted that this paper mentions that previous experimental researchers inaccurately determined the position of where the pore begins to migrate and that made comparison to theoretical models impossible.

3.6 Summary

Theoretical, experimental, and computational methods have all been used to study pore migration and have thus been investigated in preparation for the objectives of this research. Thermal gradient driven pore migration has been studied for decades and the primary driving mechanisms assumed have evolved along the way. Two basic mechanisms can be presented today that explain the phenomenon; solid-state thermodiffusion (either surface or bulk) and vapor transport. The majority of research has been focused on thermodiffusion, so much so that

no mesoscale simulation model has been developed to model pore migration in a thermal gradient due to vapor transport. This is surprising because the migration rate of large pores is dependent on the vapor transport mechanism according to the literature and these large pores, often lenticular in shape, are responsible for the development of the columnar grain structure typical of irradiated oxide based fuels. In fact, most research assumes a constant isotropic morphology during migration, which is contrary to experimental observations of multiple pore geometries (lenticular or prolate shapes). A review of pore migration research will reveal that no computer simulation has been developed that captures the characteristic change of pore shape during migration. In conclusion, there is a "void" in the relevant research for a simulation that is able to model pore migration via vapor transport and capture the drastic change in shape during migration.

CHAPTER 4

SIMULATION METHODOLOGY

4.1 Introduction

This chapter provides a basic overview for the model used in this work. It will serve to illustrate how the relevant mechanism are applied to thermal gradient driven pore migration in general and pertaining to the vapor transport mechanism. This chapter includes the theory behind the model as well as justification on why certain numerical methods were chosen. Aspects of the simulation will be discussed such as the computational domain, methods used, reduced units, and simulation initialization.

4.2 Theoretical Description

The theoretical description of the vapor-transport mechanism as given by Sens serves as a building block for the simulations developed here (Sens, 1972). A basic assumption made by Sens is that the vapor pressure of as-fabricated pores is independent of surface tension and rather a function only of temperature. This assumption can be justified by the fact that migrating pores do not remain spherical during migration. The case of constant shape would require a constant equilibrium pressure to be applied, such a case would employ $p = 2\gamma/r$ which Speight derived from thermodynamics in which p is vapor pressure, γ is the surface tension of the solid and r is the radius (see Eq. (1) in (Speight, 1964)) and is further explained by Olsen (1979). The simulation presented here employs a transport velocity equation that has been developed by Sens (see Eq. (25) in (Sens,1972)). The derivation has been previously described in section 3.2 and 3.2.3 in particular (see Eq. (3.15)). This equation allows the transport velocity of gaseous UO_2 to

be plotted against the fuel radial distance, which is shown in Figure 4.1. We assume a temperature profile to conform to a parabolic profile with a centerline temperature of 2800 K and 900 K on the outer edge. The velocity profile of UO_2 vapor can represent the pore velocity, as a function of radial position because it is assumed that vapor pressure is independent of surface tension. The microstructure features usually have a length scale that ranges from nanometers to microns and that mesoscopic scale is handled well with phase-field models; therefore, a phase-field model is believed to be well suited for illustrating the principal microstructure evolution of pore migration in a temperature gradient.

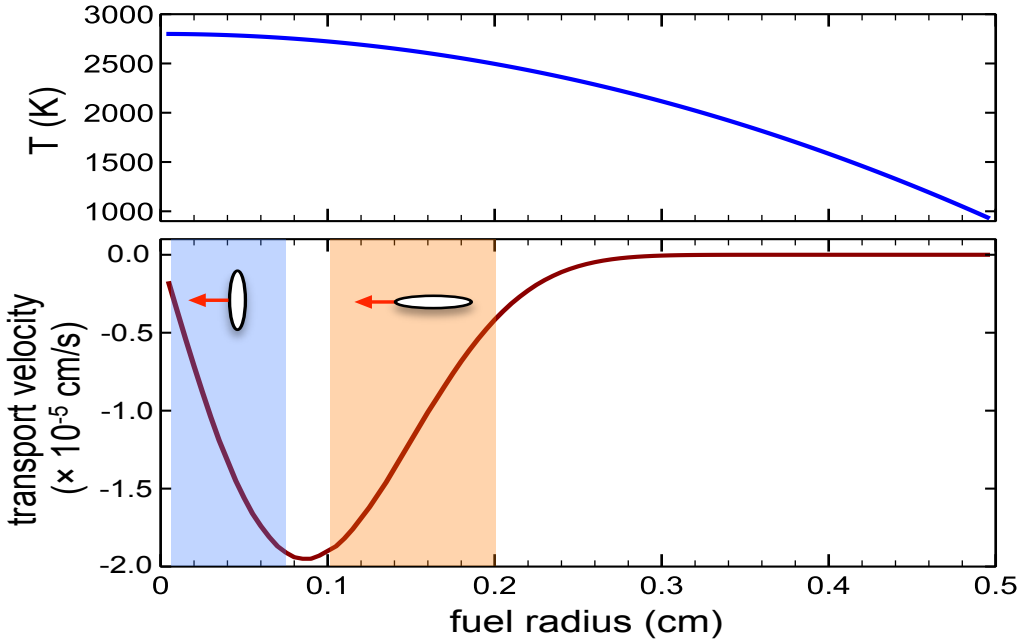

Figure 4.1. Temperature profile and graph of its associated transport velocity
The assumed temperature profile in the radial direction used in this work is shown for reference (top). The bottom figure shows the transport velocity profile for a pore due to the vapor transport mechanism as derived by Sens (1972). The transport velocity is shown as negative, which results in a migration of the pore towards the centerline of the fuel element since the positive radial direction is along the x-axis. The shaded portions of the figure show the regions of characterized pore shape morphology.

4.3 Phase Field Method

The phase-field method has become a powerful computational tool capable of modeling and predicting phenomena associated with microstructure evolution in materials. The phase-field method describes a microstructure by either using a set of conserved or nonconserved field variables that are continuous across the interfacial regions, which leads to diffuse interfaces. Interfaces can generally be categorized into two types, sharp and diffuse. Diffuse interfaces separate multiple phases with a smooth transition between values in the immediate area surrounding the interface, which is defined by a finite width. The finite width mentioned is referred to as the interfacial width and is often represented as a variable in simulations. Conventional microstructure modeling techniques use mathematically sharp interfaces to separate the compositional or structural regions. This requires the local interfacial velocity to be determined as part of the boundary conditions or calculated from the driving forces, which thus requires the explicit tracking of the interface positions. Explicit interface tracking can become complicated for systems with more than one dimension. Phase-field models can describe sharp interfaces with an infinitesimal interfacial width known as the sharp interface limit. The sharp interface description is primarily used in continuum scales while the diffuse interface is useful in mesoscale models. The variables pertaining to mobility and interface width are set to unity in this work for simplicity.

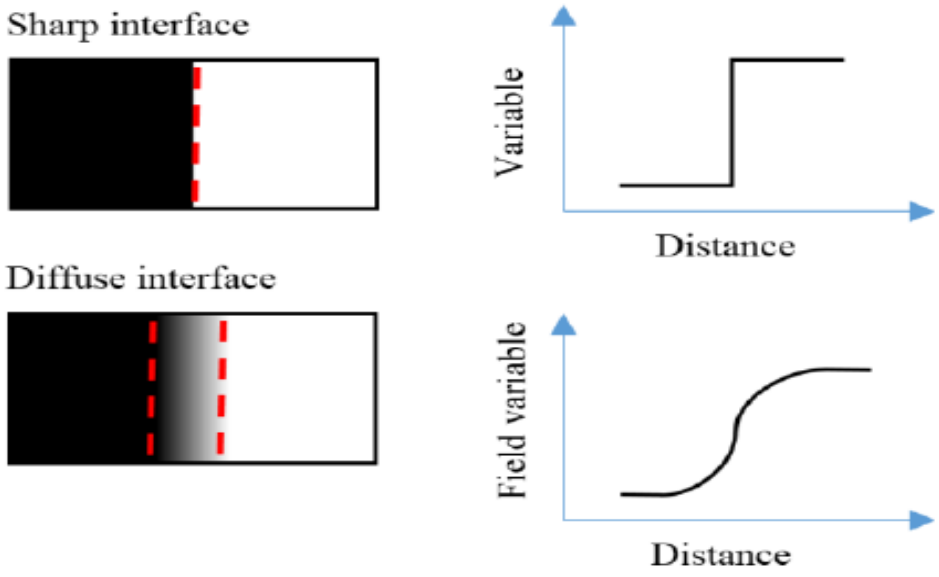

Figure 4.2. Visualization of a sharp and diffuse interface
The sharp interface (top) defines a phase as being either all of one phase or all of another with a rapid, or sharp, change between phases. The diffuse interface (bottom) allows a smooth transition between two phases (Nabi et al., 2014).

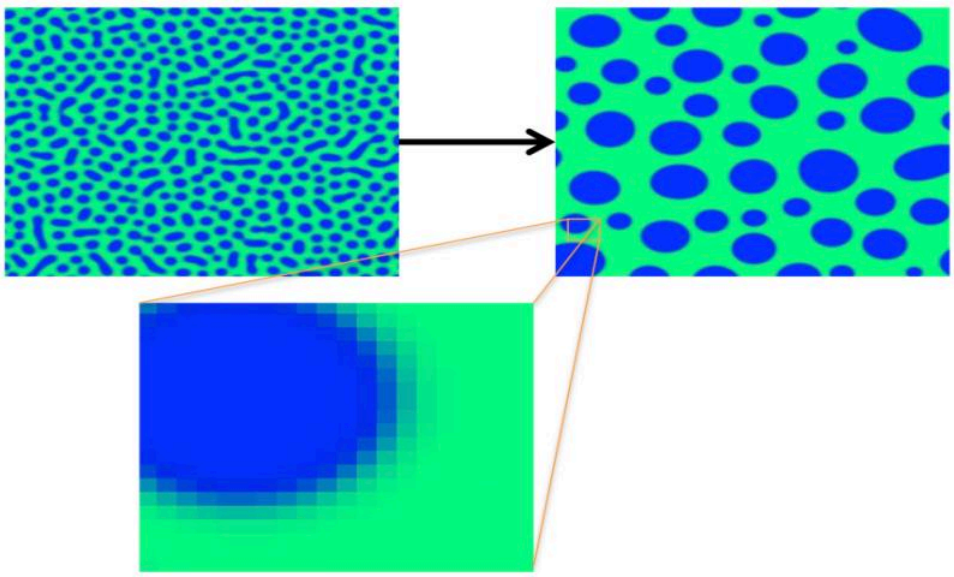

Figure 4.3. Demonstration of a diffuse interface
Simple phase-field Cahn-Hilliard simulation used to show a diffuse interface. The simulation begins with the top left picture and end with the top right picture. A portion of the final simulation frame has been expanded so that the diffuse interface can be observed.

Phase-field models substitute boundary conditions at the interface with a set of partial differential equations. This allows the model to describe the compositional/structural domains and the interfaces together with a set of field variables (Chen, 2002). Phase-field models serve to model the interface between multiple phases by observing the evolution of an auxiliary field developed from the continuous variation of field variables, also known as order parameters. Since this method does not need to explicitly track the positions of interfaces; the temporal and spatial evolution of the field variables is enough to represent the microstructure. The types of field variables, conserved and nonconserved, are governed by the Cahn-Hilliard diffusion equation and the Allen-Cahn relaxation equation, respectfully. The phase-field method uses thermodynamic and kinetic information pertaining to the simulation as an input and is then able to evolve arbitrary morphologies and microstructures. Conserved variables are so named because they conserve their integrated values globally.

4.4 Cahn-Hilliard Model

The method presented here uses the Cahn-Hilliard equation (Cahn and Hilliard, 1958) because concentration is conventionally viewed as a conserved variable. Also, phase-field models usually describe mass transport and interface migration by solid-state diffusion processes specified by the CH equation.

$$\frac{\partial c}{\partial t} = \nabla \cdot (M \nabla \mu) \tag{4.1}$$

The concentration of a chemical species is represented by the variable c and is the conserved field variable, M is the mobility of that species, and μ is the chemical potential of that species. The Ginzburg-Landau energy functional is used to describe μ:

$$\mu = \frac{\delta F}{\delta c} = \int (f(c) + \kappa |\nabla c|^2) dV \tag{4.2}$$

The free energy density associated with the chemical species, $f(c)$, is a key component of any phase-field model. The microstructure evolution of a material evolves to reduce the total free energy present and thus $f(c)$ is an important piece in determining the different phases present in the model. A double-well equation is used in this model in order to take advantage of the inherent ability of the Cahn-Hilliard equation to evolve interfacial migration within multi-phase microstructures. The double-well function represents an approximation of the Van der Waals equation of state near the critical points. A common drawback to this expression is the spontaneous drop shrinkage phenomenon that happens when the radius of a droplet is less than some critical value, but is not expected to be a problem because the initial radius is relatively large and the desired morphology will have a relatively large radius as well. It is acknowledged that more physics-based expressions could be used; such as those used by Rokkam et al. (2009) and Millett et al. (2011). However, the emphasis of the presented simulation is to explore the combined mechanisms of diffusion and advection with a driving force that leads to a migration of a pore and the double-well function is expected to perform adequately. The equation used in this model is defined as:

$$f(c) = c^2(1-c)^2 \tag{4.3}$$

The two singular points of Eq. (4.3) are c=0 and c=1 which are the concentration values used to differentiate the individual phases in the simulation. It is assumed that the variable c represents a vacancy concentration in the UO_2 material, and a pore is simply a condensation of vacancies. Therefore, the concentration within a pore is $c \approx 1$, and thus $c \approx 0$ is taken to represent the solid UO_2 material.

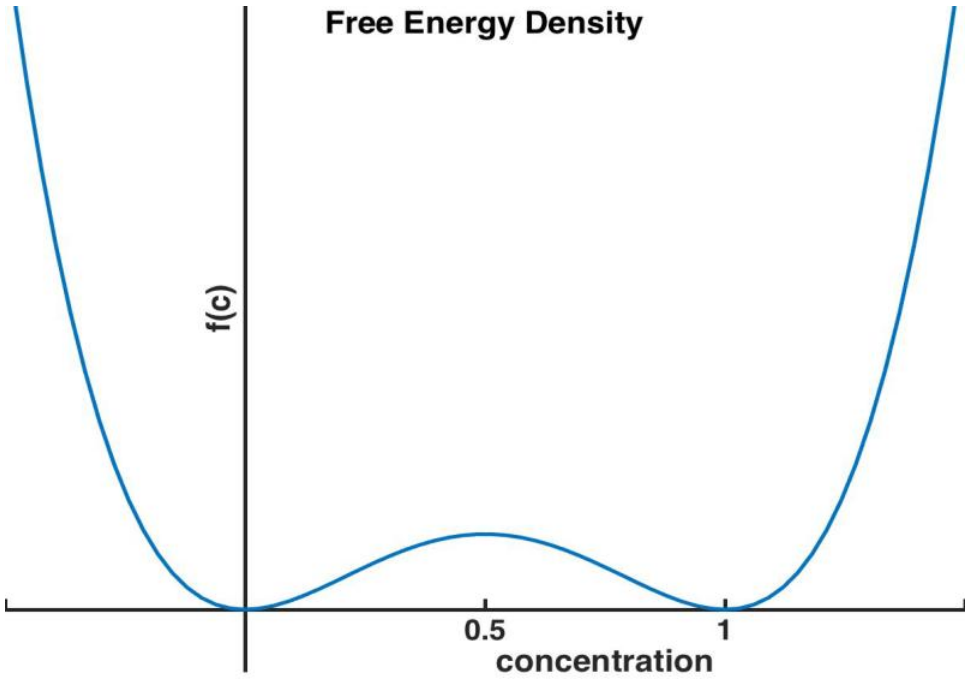

Figure 4.4. Plot of the free energy function
Plot of Eq. (4.3) in order to visualize the double well equation. Each well of the plot is considered one of the phases being modeled. Here, $c \approx 1$ and $c \approx 0$ are the two phases of the model where $c \approx 1$ corresponds to the pore and $c \approx 0$ is the fuel matrix.

4.5 Advection Equation

Another piece is still needed in order to represent vapor transport. Advection is known as the transport of a dissolved species within a convecting gas or liquid. Advection is represented as:

$$\frac{\partial c}{\partial t} = -\nabla \cdot (vc) \tag{4.4}$$

where c is the conserved concentration variable and v is a velocity field associated with the fluid that is responsible for transporting the dissolved species. Advection fits well with the idea of the vapor transport mechanism. The fuel is dissolved into a fluid, in this case a vapor, and is transported across the inside of a pore and is deposited on the opposite side. The velocity field in

this case can be represented by Sens' transport velocity equation previously described. Therefore, combining the Cahn-Hilliard diffusion equation with the advection equation to create a hybrid equation can simulate the vapor transport mechanism governing pore migration.

$$\frac{\partial c}{\partial t} = \nabla \cdot (M \nabla \mu) - \nabla \cdot (vc) \tag{4.5}$$

4.6 Solving The Cahn-Hilliard Model

The Chan-Hilliard equation can be solved or implemented in many different ways in terms of numerical methods. The method used here is the Semi-Implicit Fourier-Spectral method and will require further explanation. L.Q. Chen and Jie Shen studied the semi-implicit Fourier-spectral method used to model phase field equations. They found that this method is at least two orders of magnitude faster than explicit finite difference schemes in two dimensions with a given accuracy of 0.5% (Chen and Shen, 1998). The temporal evolution of the field variables used in phase field models is described by systems of time-dependent Ginzburg-Landau (TDGL) and Chan-Hilliard equations. Both equations are nonlinear and can only be solved numerically though discretization in space and time (Chen and Shen, 1998).

Implicit and explicit methods have both been used for obtaining numerical approximations of the CH equation. Explicit methods calculate the state of a system at a later time from the current state while implicit methods attempt to find a solution by using both the current state and a later state. The implicit method requires an extra computational step, which can be harder to implement than the explicit method. However, the explicit method can require impractically small time steps to achieve accurate results. The implicit scheme becomes more computationally efficient when large time steps are required even though it takes extra calculations. The model presented in this work deals with a physical process that requires a

relatively large time step therefore an implicit scheme is chosen. More specifically, a semi-implicit scheme is chosen. The term semi-implicit means that, in a two variable equation, one variable is treated implicitly and the other is treated explicitly. In this case the semi-implicit scheme is used to discretize the time variable used in the Ginzburg-Landau equation and a Fourier-spectral method is used to discretize the space variable.

Fourier-spectral methods are often chosen because their convergence rate is exponential in contrast to the second order convergence used by traditional finite-difference methods (Chen Shen, 1998). Fourier-spectral methods are slightly harder to implement than simpler methods and can generally only be implemented on a system with periodic boundary conditions. The basic explanation behind this type of method is that a periodic function can be represented by a series of sine and cosine functions, which in turn can be determined from a Fourier transform. A function, $p(k)$, is determined by $P(k)$ via the inverse Fourier transform as shown in Eq. (4.6).

$$p(k) = \int_{-\infty}^{\infty} P(k) e^{i2\pi kx} dk \tag{4.6}$$

where

k = wavenumber vector

$P(k)$ = forward Fourier transform of $p(x)$

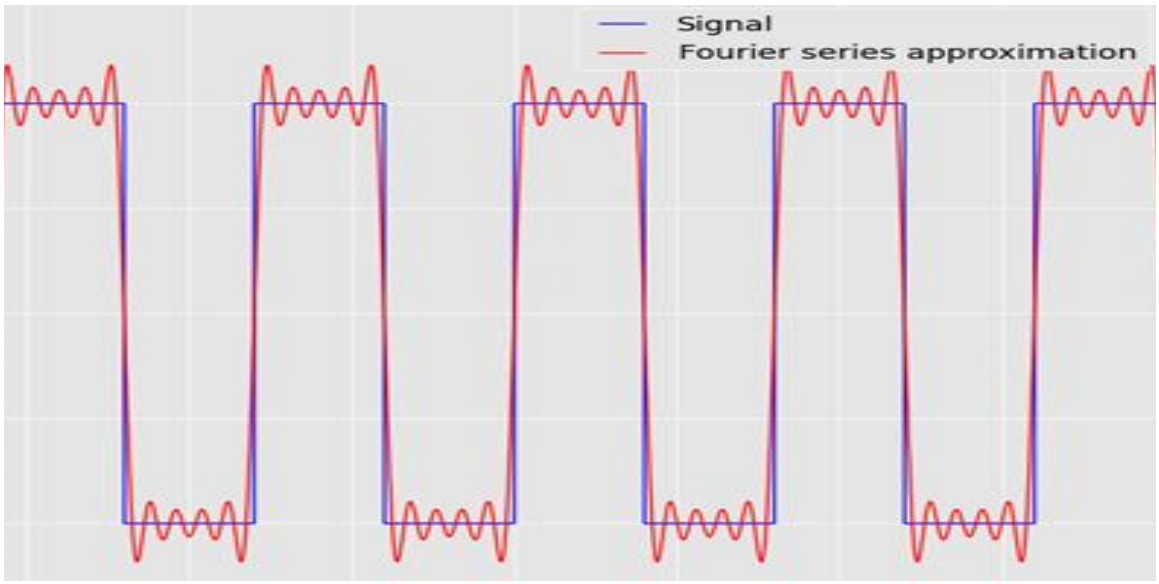

Figure 4.5. Example of a Fourier approximation
Simple visualization of a Fourier approximation of a square wave function plotted against the original function (Mic, 2015).

A Fourier transform essentially decomposes a signal into the frequencies that make it up. In practical applications, a frequency domain representation can be built that combines all the contributions of the different frequencies to recover the original function. This process is known as Fourier synthesis and is the principal behind the inverse Fourier transformation. Fourier transforms can produce relatively large errors when the original function contains discontinuities. However, they are particularly effective at approximating smooth functions such as the Cahn-Hilliard function. The Fourier-spectral method for Cahn-Hilliard equations can be seen as a two-step process developed from the work of Chen and Shen (1998). The process is: recast the Cahn-Hilliard equation in Fourier space (Eq. 4.7) and then discretize time using semi-implicit time stepping (Eq. 4.8).

$$\frac{\partial \tilde{c}(t)}{\partial t} = -Mk^2\left[\widetilde{f_0'}(c) + Kk^2\tilde{c}(t)\right] \tag{4.7}$$

$$\frac{\tilde{c}(t+dt)-\tilde{c}(t)}{dt} = -Mk^2\left[\widetilde{f_0'}(c) + Kk^2\tilde{c}(t+dt)\right] \tag{4.8}$$

Then the equation can be rearranged to get:

$$\tilde{c}(t+dt) = \frac{\tilde{c}(t) - Mk^2 \widetilde{f_0'}(c)dt}{1 + KMk^4 dt} \tag{4.9}$$

This method allows the concentration variable to be solved in Fourier space and inverted back so that the advection term can be added to the Cahn-Hilliard equation.

4.7 Implementation of The Cahn-Hilliard Diffusion-Advection Equation

The Cahn-Hilliard diffusion-advection equation, Eq. (4.5), was solved by treating the two associated terms separately. The Cahn-Hilliard diffusion term (first time on the right hand side) was solved using the semi-implicit Fourier-spectral method. The advection term is simple enough to be calculated quickly and accurately using a central finite difference approximation. Simulations were performed in the two-dimensional domain by using a uniform rectilinear mesh to represent the fuel element. A grid consisting of 512×128 nodes (or in 1024×128 nodes for some cases) was used for discretization. The larger domain is used primarily as a way of creating clear figures. Round-off errors are an unfortunate consequence of using a floating-point number system, but reduced units for length and time were chosen in order to minimize the impact of these errors. The simulations were executed with grid spacing parameters $\Delta x = \Delta y = 1.0$ and physical lengths were later assigned with $\Delta x = \Delta y = 500$ nm. The rectilinear simulation box thus represents a 256×64 μm region of the fuel, 512×64 μm for the larger simulation. The simulation is designed so that the x-direction corresponds to the radial direction and this is the direction where the velocity field gradient is applied. The time step value used during the simulations is $\Delta t = 0.1$ in reduced units, which corresponds to 4 seconds and a realistic representation of around 3.33 hours.

The transport velocity profile from Figure 1 shows two colorized regions, each corresponding to their own individual simulation. This means that two different velocity field profiles are needed; one to simulate a lenticular morphology (Eq. (4.10)) and one to simulate a prolate morphology (Eq. (4.11)). The transport velocity field is represented in reduced units as well.

$$v_x = -0.012x \tag{4.10}$$

$$v_x = 0.005x - 3.1 \tag{4.11}$$

It should be noted that $v_y = 0$ throughout the domains. The x-direction velocity fields shown in Eq. (4.10) and Eq. (4.11) are linear functions that have negative values throughout the given domain meaning that pores will always travel in the negative radial direction; i.e., towards the center of the fuel element. However, one has a negative slope and one has a positive slope. This difference in slope between Eq. (4.10) and Eq. (4.11) is expected to affect the pore shape evolution during migration. The linear velocity profiles given here can be re-scaled into physical units of centimeters and seconds where they can then be plotted and compared with Sens' model (Eq. (25) in (Sens, 1972)). Even though Sens' model is a curve, the curve can be assumed linear in the small region of the fuel element being simulated. Figure 4.6 shows this comparison below. Eq. (4.10) is shown to overlap well with the innermost region of the fuel radius and corresponds with the region from 0.0 to 0.0256 cm in the radial direction. Eq. (4.11) corresponds with the region from 0.185 to 0.2106 cm in the radial direction.

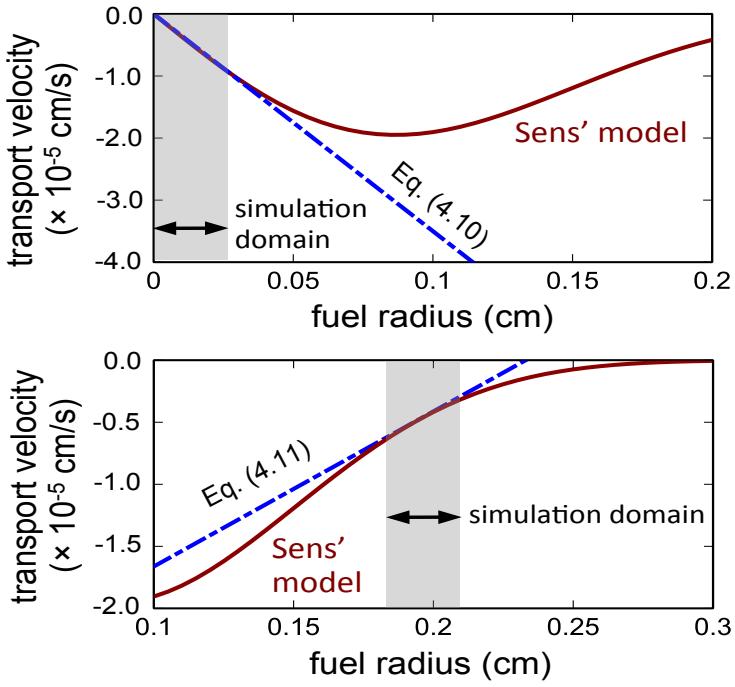

Figure 4.6. Transport velocity equation plotted with Sens' model
The linear equations used to model the transport velocity in this work are plotted over the model put forth by Sens (1972), with the top plot showing Eq. (4.10) and the bottom plot showing Eq. (4.11). Shaded regions are used in each figure to show the domain size used in their respective simulations (= 256 μm, with a 512×128 grid). It should be noted that Eq. (4.11) has been shifted to the right by 0.2 cm for this figure while keeping the slope constant.

A single pore is initialized into the simulation domain. Three morphologies are used to characterize the initial pore. The first type uses a circular pore with an initial diameter of 30 Δx corresponding to 15 μm. This size is important because it means the pore is relatively large, larger than 1 μm, and will thus have vapor transport as the driving source of pore migration. This large size is characteristic of all initial morphologies being tested in this work. The second type of morphology being used is an ellipsoid. Two types of ellipsoids are being used; one that has an aspect ratio of five to one and another whose aspect ratio is one to five. All three initial morphologies will be simulated with each velocity field previously described for a total of six simulations; each shape with Eq. (4.10) and each shape with Eq. (4.11). The pore center is

located at the point 480×64 for the smaller simulation domain and 900×64 for the larger domain. This location corresponds to the cold side of the domain since x = 0 is the portion of the simulation domain that is closest to the fuel centerline. For example, the simulation domain used in association with Eq. (4.10) is adjacent to the centerline of the fuel, meaning that x = 0 is the centerline and x = 512 or 1028 in the radial direction is the opposite end of the simulation domain. All simulations are run for 3000 time steps.

CHAPTER 5

RESULTS AND DISCUSSION

5.1 Introduction

The simulations and figures presented here characterize the migration of a single pore in a temperature gradient. Multiple initial morphologies are used during the course of these simulations in order to demonstrate the change in shape that occurs during migration. The pore is shown to migrate in the direction of the temperature gradient towards the centerline of the fuel, which is in agreement with both theoretical predictions and experimental observations. Changes to the pore's shape during migration were also captured during the simulation and both lenticular and bullet shapes were observed. Pore migration is also shown to be due to the vapor transport mechanism and not the thermodiffusion mechanism used by other models. A contour field was created as to visualize the advection flux and vacancy concentrations present in the simulation. Differences in the shape morphology of migrating pores could potentially cause the pore's migration velocity to deviate. A parametric study was built to monitor the pore's migration velocity and compare it to the prescribed transport velocity equation. Since dimensional changes were observed in the migrating pores; it is worthwhile to calculate those changes and create a figure to show dimension change versus pore position.

5.2 Shape Morphology

The initial morphologies that will be shown include a circle, an ellipse with a five to one aspect ratio, and another ellipse with an aspect ratio of one to five. In the case of the circular

pore, an initial diameter of 30 Δx, which corresponds to 15 μm in physical units is used. This diameter places the pore well above the theoretical "large" category where vapor transport is the dominant mechanism responsible for migration. Any contribution to an overall migration velocity due to solid-state thermodiffusion will be negligible, and thus vapor transport is the only driving mechanism considered for the simulation. The following figures were taken from the simulations that used the larger grid; a 1024×128 grid. Therefore, discussion on the simulations will be limited to as it pertains to the larger grid. All initial pores are placed at x = 900 Δx and y = 64 Δy. The simulation domain is oriented so that the hottest portion, center, of the fuel element is located on the left hand side.

Figure 5.1- 5.3 uses Eq. (4.10) as the supplied transport velocity equation. The use of Eq. (4.10) means the simulation domain corresponds to a region immediately adjacent to the centerline of the fuel; the fuel centerline is at the left end of the domain and the right end of the domain corresponds to a point 512 μm into the radial direction. These figures depict successive snapshots of a pore as it migrates across the domain in the x-direction. Migration of the pore in this direction is in agreement with the literature because pore migration should always be in the direction of increasing temperature; i.e. toward the centerline of the fuel element. The x-component of the velocity field is negative throughout the domain, which results in a pore that migrates in the negative x-direction. This orientation is similar to the axial definition of Figure 4.1. The most notable aspect of Figure 5.1 is the transformation of the pore from a circle to a lenticular shape during the migration process. This morphological change is due to the slope of the transport velocity equation in the x-direction (see Figure 4.6). The equation, Eq. (4.10), produces a negative velocity profile and has a negative slope throughout the domain. This causes the leading surface of the pore to experience a lower (or, less negative) velocity than the

trailing surface. This results in the trailing edge moving slightly faster than the leading edge of the pore and thus reduces the width of the pore in the x-direction and the formation of a lenticular shape. The concentration parameter, c, and the volume of the pore remain conserved due to the characteristics of the prescribed phase field model. The surface area of the pore increases as the x-direction width approaches zero and counters the kinetic driving force for pore shape change previously described, which prevents the pore's width from reducing to zero. The pore then reaches a steady-state lenticular morphology.

Figure 5.1 shows 4 snapshots of the simulation that are taken at equally spaced intervals of time, with the top image corresponding to the beginning of the simulation and the bottom image corresponding to the end. Monitoring the relative position of the pore at each instance in time allows for the deduction that the pore velocity is highest at initial stages of the simulation. The velocity begins to decrease as the pore approaches the left side of the domain and the end of the simulation. This type of behavior is expected because the velocity field defined by Eq. (4.10) equals zero at the left side of the domain.

Figure 5.2 shows 4 snapshots of the simulation at equally spaced intervals of the simulation. This particular simulation is for the initial ellipsoid morphology with an aspect ratio of five to one. This simulation is able to show a pore with an initial morphology similar to the prolate shape transforming into a lenticular morphology during migration.

Figure 5.3 depicts snapshots for the initial ellipsoid morphology with an aspect ratio of one to five. The pore in this simulation is initially the lenticular shape that is expected to occur at the end of the simulation. Therefore, the figure simply shows and ending morphology that is very similar to the beginning shape of the pore.

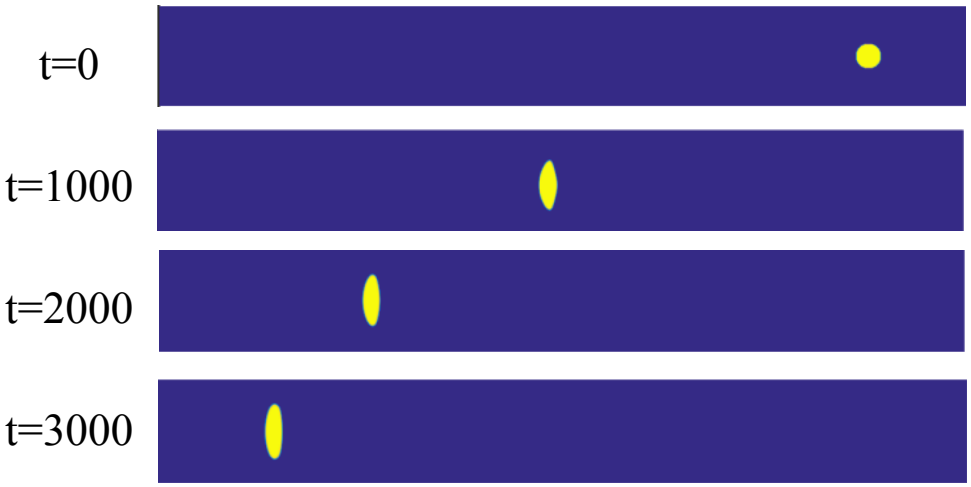

Figure 5.1. Pore migration simulation using Eq. (4.10) and starting from a circle
Snapshots of a simulation showing pore migration when using Eq. (4.10). The images are arranged top-to-bottom and correspond to 0, 1000, 2000, and 3000 simulation steps, respectively. The left side of the simulation domain corresponds to the fuel centerline. These images were taken from a simulation that used the larger grid (1024×128).

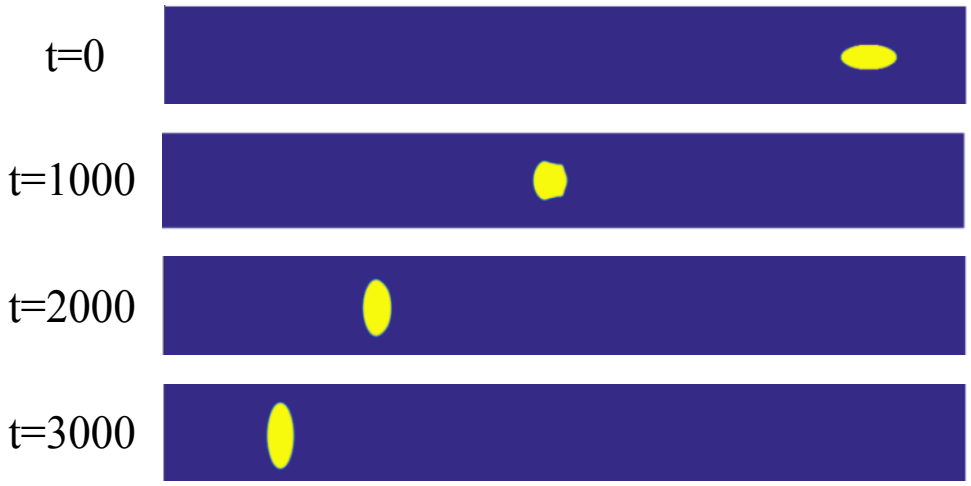

Figure 5.2. Pore migration simulation using Eq. (4.10) and starting from a 5:1 ellipsoid
Snapshots of a simulation showing pore migration when using Eq. (4.10). The images are arranged top-to-bottom and correspond to 0, 1000, 2000, and 3000 simulation steps, respectively.

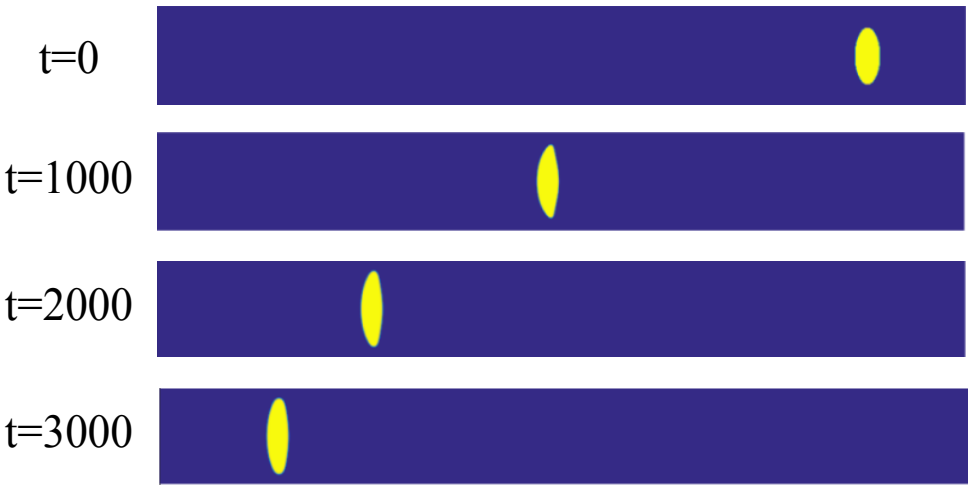

Figure 5.3. Pore migration simulation using Eq. (4.10) and starting from a 1:5 ellipsoid Snapshots of a simulation showing pore migration when using Eq. (4.10). The images are arranged top-to-bottom and correspond to 0, 1000, 2000, and 3000 simulation steps, respectively.

The second set of simulations used Eq. (4.11) as the prescribed transport velocity equation. Figure 5.4- 5.6 shows snapshots of the simulations in the same manner as above. The transport velocity here, much like of Eq. (4.10), consists of negative values throughout the domain that cause pore migration in the negative x-direction. However, this time the velocity field has a positive slope in the x-direction. This causes the leading edge of the pore surface to experiences a larger velocity than the trailing edge. The pore will then elongate in the x-direction and become similar to the experimentally observed prolate shape.

The type of velocity field caused by Eq. (4.11) induces a pore shape transformation from a circular shape into a prolate (bullet) shape for Figure 5.4. It is observed that a somewhat circular protrusion develops at the leading surface of the pore and continues to evolve during migration.

Figure 5.5 uses an elliptical pore with an aspect ratio of five to one. The pore has an initial shape similar to the prolate morphology expected to occur during the simulation. The

positive slope induced by Eq. (4.11) causes the pore to elongate in the x-direction as expected. The elongation present in Figure 5.5 is much greater than in Figure 5.4 due to the pore initially being in the prolate orientation.

Figure 5.6 is for the simulation using an initial elliptical shape with an aspect ratio of one to five. The pore began to precipitate during the simulation and resulted in a pore that was breaking up as the simulation progressed. However, it can be observed that the pore began to approach a circular shape during the simulation, which is similar to the behavior of Figure 5.2. This circular shape is a key step in transforming between morphologies; from a lenticular shape to a prolate shape in this case. The prolate morphology is a result of the leading edge moving faster than the trailing edge of the pore, and the nucleation action here is believed to be a result of this leading edge moving too fast for the concentration available. Therefore, adjustments would need to be made to the simulation variables to fully capture the lenticular to prolate shape transformation, but the precipitation in Figure 5.6 is not of major significance.

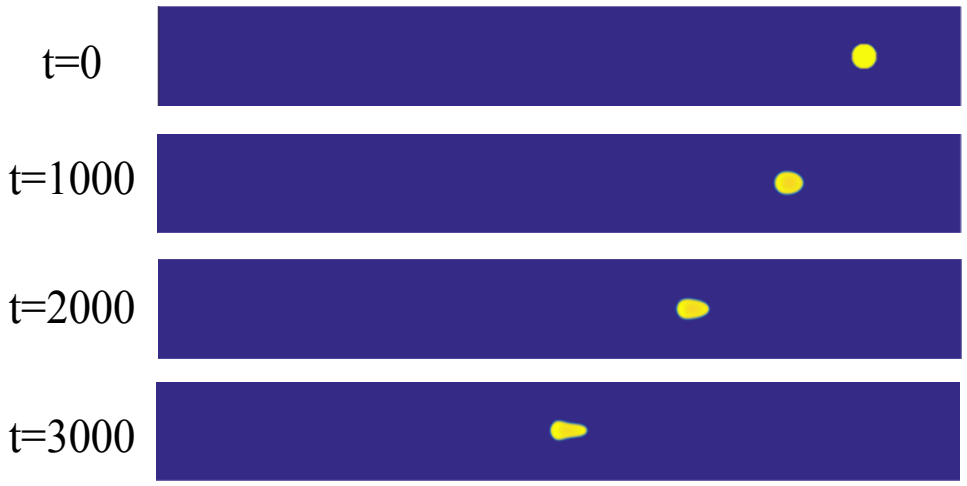

Figure 5.4. Pore migration simulation using Eq. (4.11) and starting from a circle
Snapshots of a simulation showing pore migration when using Eq. (4.11). The images are arranged top-to-bottom and correspond to 0, 1000, 2000, and 3000 simulation steps, respectively. These images were taken from a simulation that used the larger grid (1024×128).

Figure 5.5. Pore migration simulation using Eq. (4.11) and starting from a 5:1 ellipsoid
Snapshots of a simulation showing pore migration when using Eq. (4.11). The images are arranged top-to-bottom and correspond to 0, 1000, 2000, and 3000 simulation steps, respectively. These images were taken from a simulation that used the larger grid (1024×128).

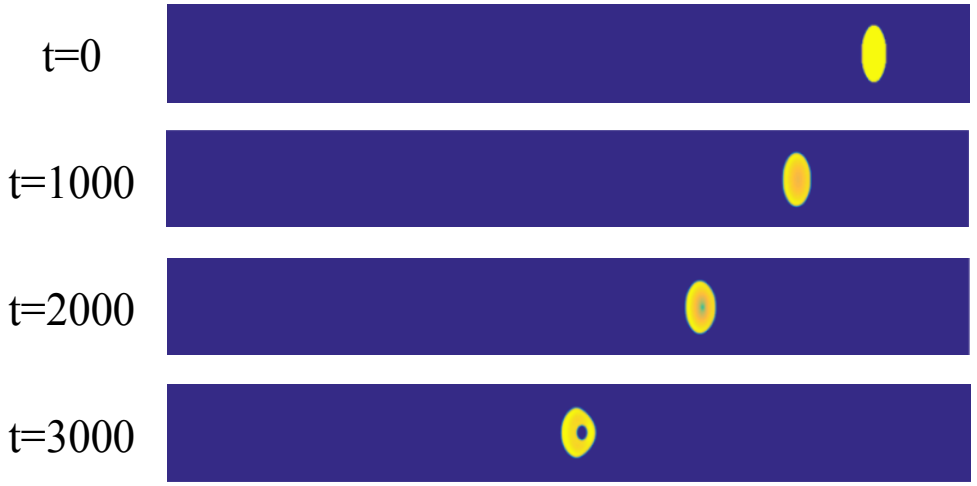

Figure 5.6. Pore migration simulation using Eq. (4.11) and starting from a 1:5 ellipsoid
Snapshots of a simulation showing pore migration when using Eq. (4.11). The images are arranged top-to-bottom and correspond to 0, 1000, 2000, and 3000 simulation steps, respectively. These images were taken from a simulation that used the larger grid (1024×128).

5.3 Contour Plot

The primary simulations in this work are mainly performed to demonstrate pore shape change during migration. A contour plot was built in order to better understand the spatiotemporal evolution of both the pore shape and the advection flux present during simulation. Figure 5.7a-5.7c shows a close up view of a pore during the lenticular simulation with intervals akin to those of Figure 5.1 without the initial position snapshot. A contour field is used to represent the vacancy concentration and an overlaid vector field is used to represent the advection flux. Figure 5.7d is an even closer view of the shaded box from Figure 5.7b to better visualize the advection flux field. Figure 5.7d shows the advection flux as vector arrows and it can be seen that the advection flux only exists to any significance within the interior of the pore. The length and direction of the vectors represent the flux of vacancies within the pore and are equal and opposite to the flux of the solid UO_2 fuel material. This means that solid material is being moved from the hot surface of the pore to the cold surface of the pore, which depicts the vapor transport mechanism.

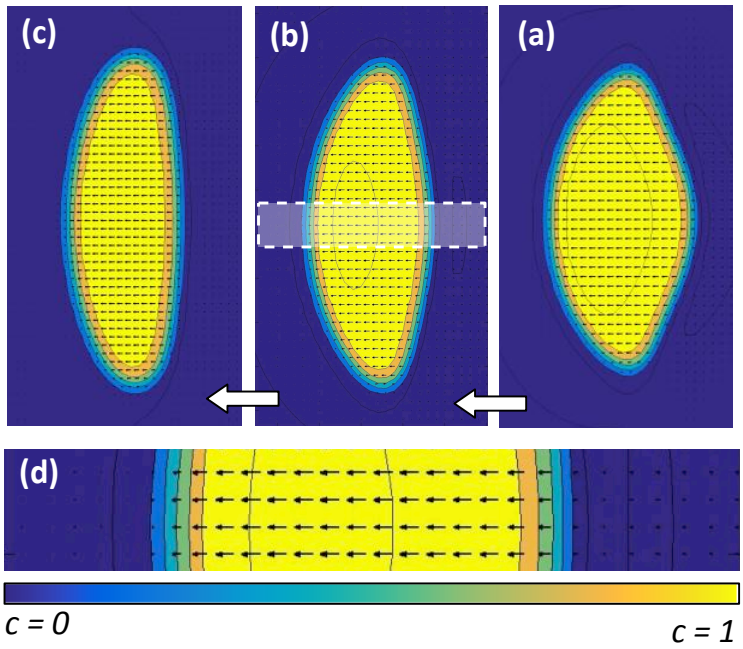

Figure 5.7. Contour plots showing advection flux for the lenticular pore
Images (a), (b), and (c) illustrate the pores shape at different instances in time for the lenticular profile achieved using Eq. (4.10). A vector plot is overlaid in order to depict the advection flux present due to vapor transport. The magnified view (d) corresponds to the shaded box in (b). The lengths of the vectors are proportional to the magnitude of flux and are only significant within the pore.

5.4 Parametric Study

Research by Nichols (1972) concluded, based on mathematically derived relations that the velocity of a migrating pore due to the vapor transport mechanism does not depend on the pore's shape. Therefore, it is necessary to study the velocity of a migrating pore during the simulation to see if changes to the pore shape resulted in a deviation of the pore velocity from the prescribed transport velocity equation.

The instantaneous position of the pore's 'center of mass' was calculated by averaging the x- and y-positions of all the grid points with a concentration value of $c > 0.5$. The position points were plotted against the simulation time. The plot subsequently allowed for the pore's

instantaneous velocity to be calculated using a finite-difference approximation for the derivative of the pore position versus the time curve. The pore velocity was then plotted against the pore's x-position (i.e., the pore's radial position). The pore transport velocity for the lenticular profile, as modeled by Eq. (25) from Sens' work and seen in Figure 4.1, was then overlaid so that comparisons can be made. The results for the simulations using Eq. (4.10) are shown Figure 5.8-5.10 which corresponds to the simulations performed and shown in Figure 5.1-5.3; the pore's velocity matches very closely with the imposed transport velocity model throughout the simulation, despite the fact that the pore has drastically changed its shape during migration and despite different initial morphologies. A small difference between simulation and prescribed equation can be observed at the beginning stages of the simulation, at the right hand side of Figure 5.8-5.10, but this is believed to be due to an initial acceleration that the pore must perform since the pore has an initial velocity of zero.

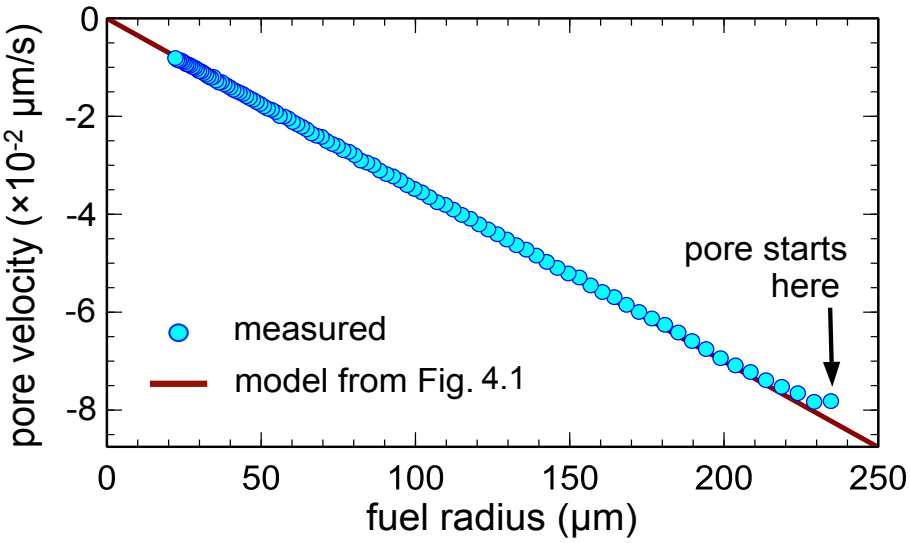

Figure 5.8. Simulated migration velocity using Eq. (4.10) and starting from a circle
The velocity of a migrating pore is plotted versus the pore's radial position. Blue data points correspond to the velocity values measured from the simulation that used Eq. (4.10). The red line corresponds to Eq. (4.10). The figure shows that even though the pore has changed shape to a lenticular morphology, the pore velocity matches very closely to the prescribed model.

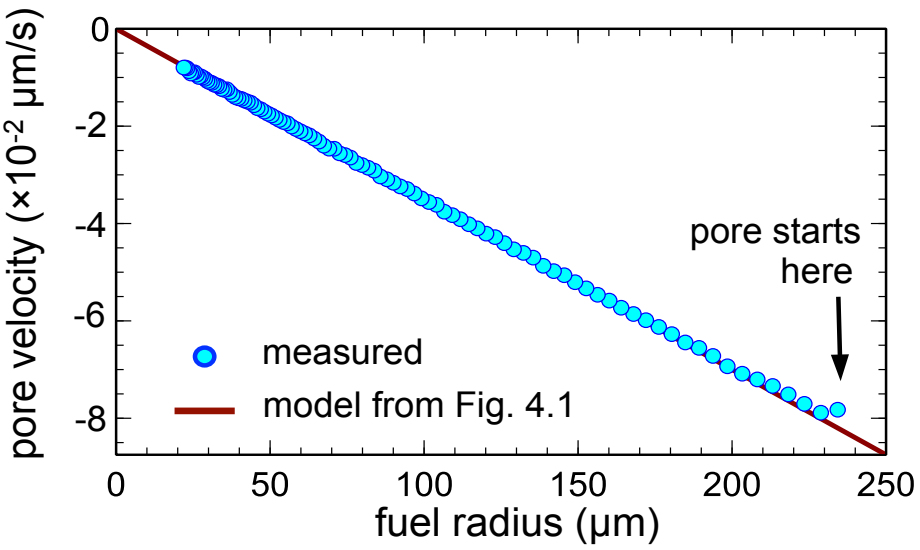

Figure 5.9. Simulated migration velocity using Eq. (4.10) and starting from a 5:1 ellipsoid
The velocity of a migrating pore is plotted versus the pore's radial position. Blue data points correspond to the velocity values measured from the simulation that used Eq. (4.10). The red line corresponds to Eq. (4.10).

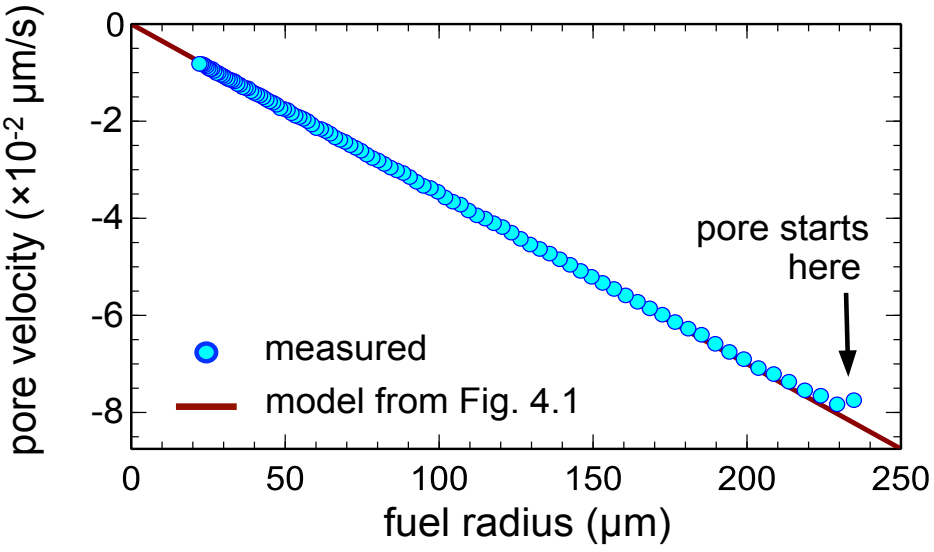

Figure 5.10. Simulated migration velocity using Eq. (4.10) and starting from a 1:5 ellipsoid
The velocity of a migrating pore is plotted versus the pore's radial position. Blue data points correspond to the velocity values measured from the simulation that used Eq. (4.10). The red line corresponds to Eq. (4.10).

The same process described above was repeated for the prolate (bullet) simulations when the transport velocity of Eq. (4.11) was used, and the results are shown in Figure 5.11-5.13. These figures correspond to the simulations shown in Figure 5.4-5.6. The results show that the pore velocity from the simulation matches closely with the associated transport velocity model throughout the simulation.

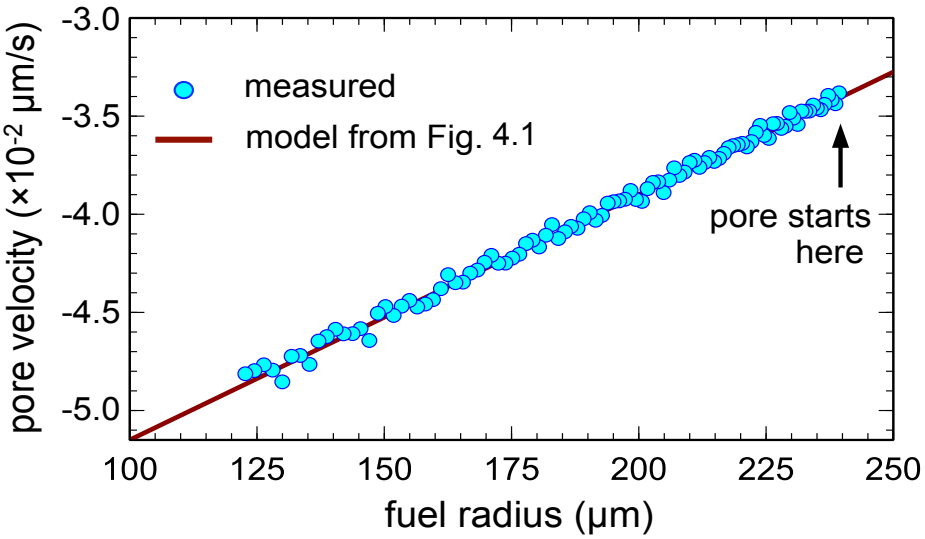

Figure 5.11. Simulated migration velocity using Eq. (4.11) and starting from a circle
The measured velocity of a migrating pore for the simulation using Eq. (4.11) is shown with blue data points and is plotted over the red line, which corresponds to Eq. (4.11). The velocities are plotted against the pore's radial position. The simulation shows a pore that transformed into a prolate (bullet) shape and this figure shows that the velocity profile during the simulation still matches closely with the prescribed equation.

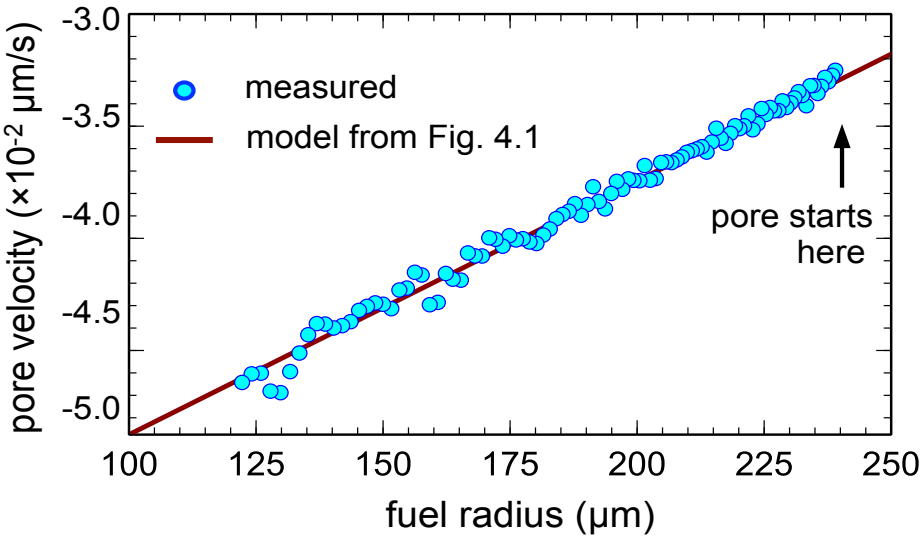

Figure 5.12. Simulated migration velocity using Eq. (4.11) and starting from a 5:1 ellipsoid
The measured velocity of a migrating pore for the simulation using Eq. (4.11) is shown with blue data points and is plotted over the red line, which corresponds to Eq. (4.11). The velocities are plotted against the pore's radial position. The simulation shows a pore that began in a prolate orientation and extended axially throughout the simulation.

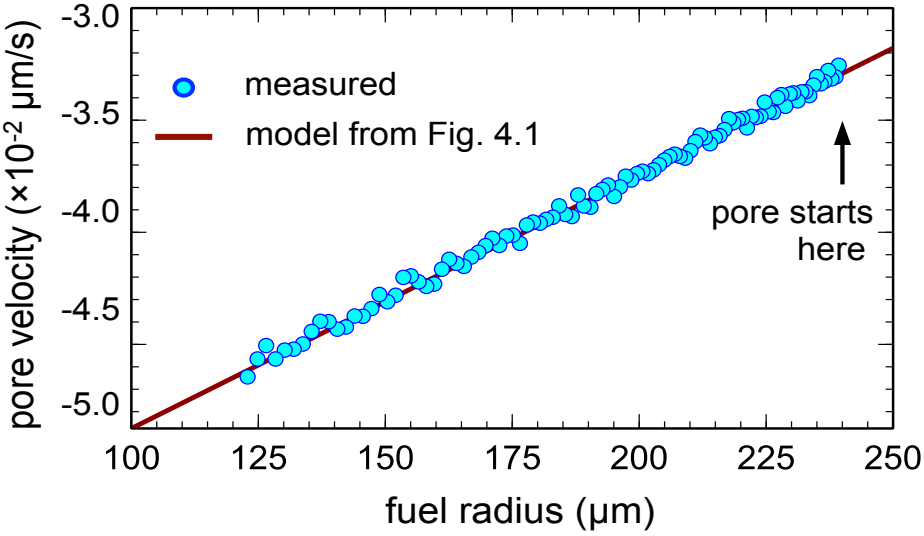

Figure 5.13. Simulated migration velocity using Eq. (4.11) and starting from a 1:5 ellipsoid
The measured velocity of a migrating pore for the simulation using Eq. (4.11) is shown with blue data points and is plotted over the red line, which corresponds to Eq. (4.11). The velocities are plotted against the pore's radial position. The simulation shows a pore that began as in a lenticular orientation.

The results of this study serve to conclude if pore shape influences transport velocity. Simulations were performed that showed drastic changes in pore shape during migration for both lenticular and prolate morphologies. The instantaneous velocities of the pore during the simulations closely followed that of their respective prescribed transport velocity models thus showing that shape did not affect velocity during these simulations. This illation is in agreement with the work previously performed by Nichols (1972).

5.5 Dimensional Changes

One of the primary objectives of this work is to demonstrate a pore's change in shape during migration. Figures 5.1-5.6 show this change in shape during the simulation, but the dimensional changes observed still need to be described numerically to fully understand the changes in morphology. The dimensional changes in the migrating pores were calculated for each simulation. The pore's width in the x- and y-directions were calculated and plotted versus the pore's radial position in order to visualize how much the pore has changed in each dimension and where the change occurs.

In the case of initially circular pores, both pores began as 15 μm circular pores. The end of the simulation shows that the lenticular pore, using Eq. (4.10), reached x- and y-dimensions of 10.5 and 31.5 μm, respectively. The prolate simulation, using Eq. (4.11), ended with x- and y-dimensions of 30.0 and 9.5 μm, respectively. These results can be seen in Figure 5.14, for both the lenticular simulation and the prolate simulation. The only difference between the two types of simulations is the attributed values for the transport velocity. Therefore, the transport velocity equation assigned (and its mathematical properties such as radial profile, slope, and sign of slope) is the important parameter that dictates the change in pore shape during migration.

The initial elliptical morphologies are shown in Figure 5.15 and Figure 5.16. Figure 5.15 uses Eq. (4.10) as the prescribed transport velocity equation. This figure is able to portray the change in shape from a prolate like initial morphology into a lenticular morphology well because the pores width in the x- and y-directions can be seen crossing each other and then continue to evolve (top). It also demonstrates than an initial lenticular shape will maintain its shape as the simulation progresses (bottom). Figure 5.16 uses Eq. (4.11) as the prescribed velocity equation. It demonstrates that an initial prolate shape will maintain its overall shape as it evolves during migration (top). It also shows an initial lenticular morphology attempting to become a prolate morphology by showing the pores width in the x- and y-directions converging on each other, similar to the top of Figure 5.15 (bottom).

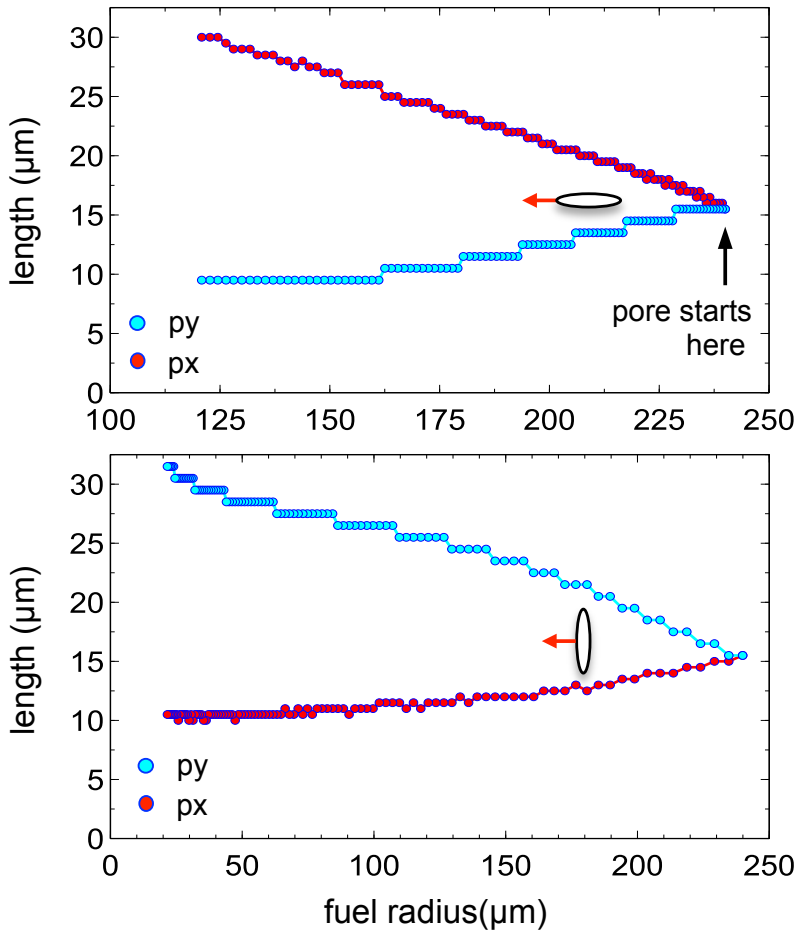

Figure 5.14. Plots showing the shape evolution of a circular pore during migration
The x- and y-dimensions of a migrating pore are plotted against the fuel radius. The top figure is for the simulation using Eq. (4.11) and shows the transformation of a pore into a prolate morphology. The bottom figure shows data for the simulation using Eq. (4.10) and demonstrates a transformation from an isotropic morphology into a lenticular morphology. The blue dots correspond to the pore's y-dimension and the red dots correspond to the pore's x-dimension.

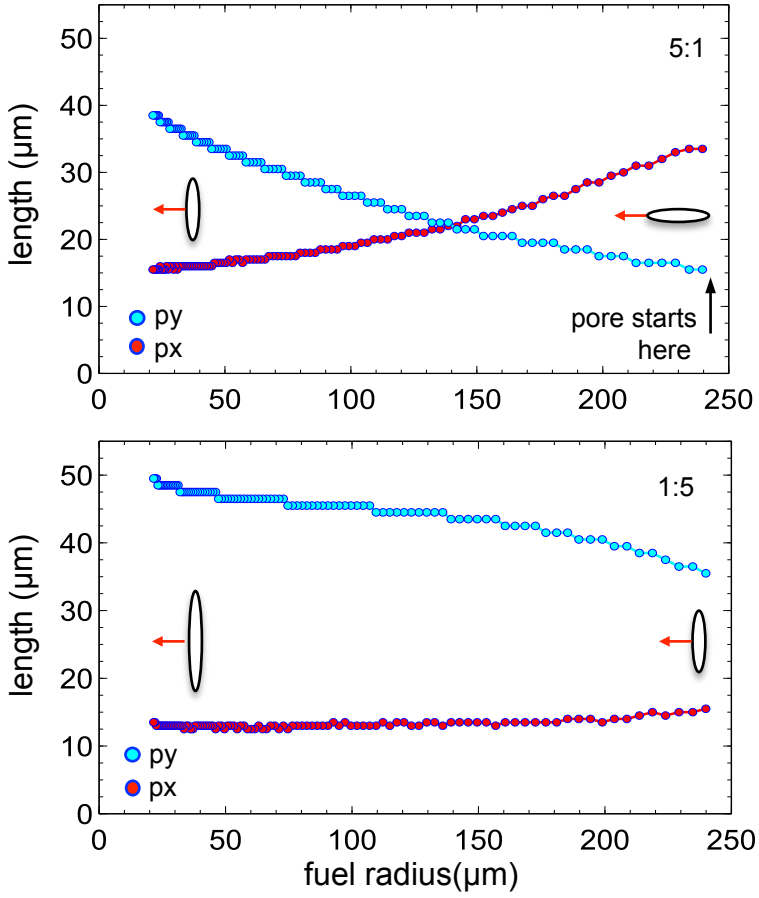

Figure 5.15. Shape evolution of an initial ellipsoid during migration using Eq. (4.10)
The x- and y-dimensions of a migrating pore are plotted against the fuel radius. The top figure is for the simulation using an ellipsoid with an aspect ratio of 5:1 and the bottom figure is for the ellipsoid with an aspect ratio of 1:5. Both figures presented here use Eq. (4.10) as the prescribed transport velocity profile. The blue dots correspond to the pore's y-dimension and the red dots correspond to the pore's x-dimension.

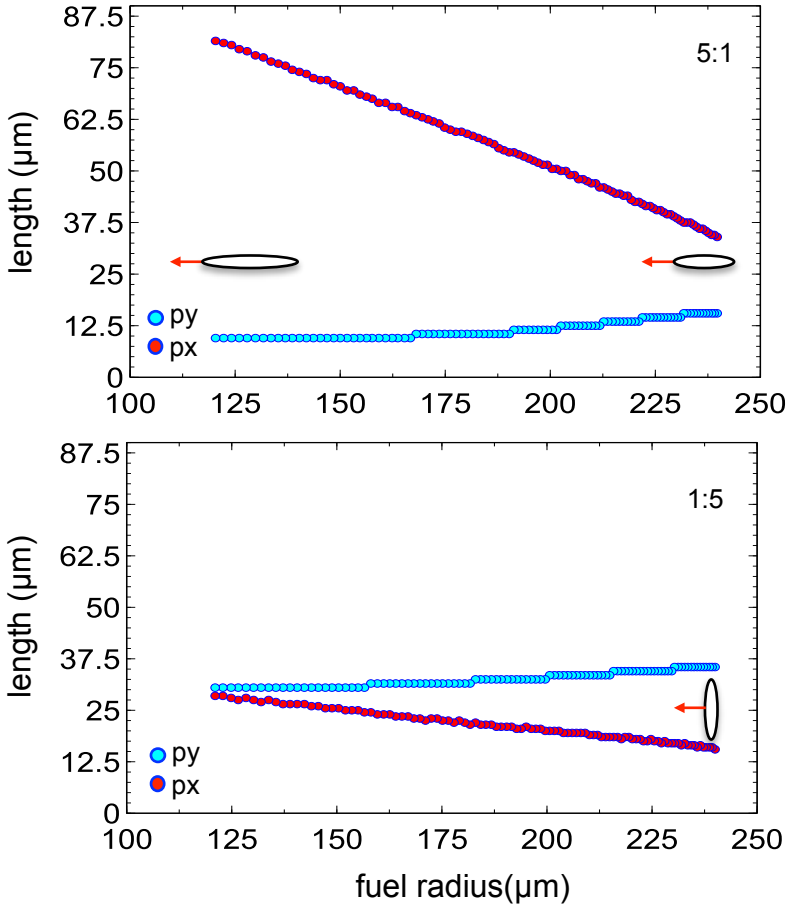

Figure 5.16. Shape evolution of an initial ellipsoid during migration using Eq. (4.11)
The x- and y-dimensions of a migrating pore are plotted against the fuel radius. The top figure is for the simulation using an ellipsoid with an aspect ratio of 5:1 and the bottom figure is for the ellipsoid with an aspect ratio of 1:5. Both figures presented here use Eq. (4.11) as the prescribed transport velocity profile. The blue dots correspond to the pore's y-dimension and the red dots correspond to the pore's x-dimension.

CHAPTER 6

CONCLUSION

6.1 Summary

A computational simulation of pore migration in a thermal gradient due to the vapor transport mechanism has been performed using phase-field modeling techniques. The simulation presents the vapor transport mechanism as UO_2 molecules diffuse through the pore interior due to a temperature gradient. The model utilizes the traditional Cahn-Hilliard equation appended with an advection term to create an equation that requires a vapor transport velocity field to be supplied and thus model the vapor transport mechanism. Two simple linear velocity profiles were used during the course of this thesis to be the supplied vapor transport velocity fields. The two simple equations were closely correlated to the transport velocity equation developed by Sens (1972) at two different radial positions within the fuel. The simulations performed show the migration of a single large pore across the simulation domain. These simulations illustrate highly non-equilibrium shapes, lenticular and prolate geometries, forming during their migration toward the hot side of the fuel. The dimensional changes of the pore during migration were closely monitored because experimental observations state that highly non-equilibrium shapes have been observed during migration. The pore migration velocity was also closely tracked so that it could be compared to the supplied velocity equations.

In summary, a phase-field model was built that incorporates thermal gradient-driven migration of pores in oxide fuel due to the vapor-transport mechanism. The model developed successfully showed migration of a pore towards the end of the simulation domain that represented the centerline of the fuel and thus the hottest portion of the fuel. An initially isotropic pore demonstrated concurrent changes in shape during its migration. Elliptical initial

shapes were also simulated that showed concurrent changes in shape during migration as well. Moreover, both lenticular and prolate morphologies were observed and the predicted morphology was shown to be in agreement with changes to the supplied transport velocity equation. Also, the velocity of the pore during migration accurately represented the supplied transport velocity equation and changes to the pore's shape during migration did not influence its velocity (i.e., migration velocity is independent of shape). The behavior of the model in terms of the transport mechanism, pore shape change, migration direction, and velocity independence is all in agreement with related literature. A model that successfully shows changes in shape morphology and migration due to the vapor transport mechanism is being presented for the first time.

6.2 Conclusions

The simulations presented here illustrate that the slope of the transport velocity field can explain the non-equilibrium shapes, lenticular and prolate geometries, observed in migrating pores. Figures 5.1 demonstrates a lenticular morphology and Figure 5.4 shows a prolate geometry for the isotropic initial pore. The only difference between the simulations shown in these figures is the supplied transport velocity equation, and the slope of the transport velocity field in the radial direction describes the difference between Eq. (4.10) and Eq. (4.11). Therefore, it can be concluded that the slope of the transport velocity field is responsible for the change in a pore's shape during migration. Consequently, this information gives additional support to the notion of large pore migration during fuel restructuring being driven by the vapor transport mechanism. This conclusion draws from the fact that similar simulations of large pore

migration via solid-state thermodiffusion do not show any change to the pore's shape during its migration (Hu and Henager, 2010)(Li et al., 2010)(Zhang et al., 2012).

Additionally, it was found that the magnitude of a migrating pore's velocity in these simulations is independent of any changes in shape that occur based on the information presented in Figure 5.8 and Figure 5.11. This conclusion agrees with the work of Nichols (1972) who states that the velocity of a pore migrating due to the vapor transport mechanism is independent of changes to the pore's shape. However, Sens' model contains a built in assumption that the internal vapor pressure of the pore is a function solely based on temperature and therefore neglects contribution from surface tension. It was not investigated whether or not this assumption affects the previous conclusion.

6.3 Recommendations For Future Work

The model and simulations presented in this thesis successfully reproduce the transformation of an initially isotropic pore into either a lenticular or prolate shape via the vapor transport mechanism, and it is believed to be an advance over other recent attempts to simulate thermal-gradient-driven pore migration (Li et al., 2010)(Zhang et al., 2012)(Tikare and Holm, 2005). This type of work is used to help understand the mechanism of vapor transport behind thermal gradient driven migration in large pores with the hopes of engineering microstructures for optimal performance of the fuel. This model could potentially, for this reason, lead to significant scientific progress if it is further refined.

A more sophisticated version of this model could include a direct calculation of the spatially dependent temperature field surrounding the pore (in the fuel element), and allow that to inform the transport velocity field. The current model presented here assumes a particular

temperature profile when the transport velocity field was assigned. Though this was a rather simple way of dealing with this variable, it was sufficient for the purpose of this work. This work also only used a single pore in the simulations. Future models could include the migration of multiple pores in a polycrystalline matrix in order to understand the formation of the columnar grain structure. Additional pores could also mean supplementary physics to handle pore coalescence. Further work on this particular model could also investigate if surface tension forces will affect the conclusion of velocity independence stated earlier.

REFERENCES

Allen, S. M., Cahn, J. W., 1979, “A microscopic theory for antiphase boundary motion and its application to antiphase domain coarsening,” *Acta Metallurgica*, Vol. 27, pp. 1085-1095.

Cahn, J.W., Hilliard, J.E., 1958, “Free Energy of a Nonuniform System,” *The Journal of Chemical Physics*, Vol. 28, pp. 258–267.

Chen, L.Q., Shen J., 1998, "Applications of Semi-implicit Fourier-spectral Method to Phase Field Equations," *Computer Physics Communications,* 108, pp. 147-58.

Chen, L.Q., 2002, "Phase-Field Models for Microstructure Evolution," *Annual Review of Materials Research*, Vol. 32, pp. 113-40.

Denbigh, K. G., 1950, “The Thermodynamics of the Steady State,” Methuen, London.

Desai, T.G., et al., 2010, "Atomistic Simulations of Pore Migration under Thermal Gradient in UO2," *Acta Materialia*, Vol. 58, pp. 330-39.

Dushman, S., 1958, “Scientific Foundations of Vacuum Technique,” Wiley, New York, pp. 75.

Halas, D.R. De, Horn, G.R., 1963, "Evolution of uranium dioxide structure during irradiation of fuel rods," *Journal of Nuclear Materials*, Vol. 8, pp. 207-220.

Hu, S.Y., Henager, C.H., “Phase-field simulation of pore migration in a temperature gradient.” *Acta Materialia*, Vol. 58, pp. 3230-3237.

Kaneko, H., et al., 1969, “Calculation Program MIPORE for Structure Change of Oxide Fuel during Irradiation,” *Journal of Nuclear Science and Technology*, Vol. 6, pp. 601-603.

Kawamata, H., et al., 1977, “Migration Rate of Lenticular Pores in UO2 Under the Influence of Temperature Gradient,” *Journal of Nuclear Materials*, Vol. 68, pp. 48-53.

Li, Y., et al., 2010, “Phase-field modeling of pore migration and growth kinetics in materials under irradiation and temperature field,” *Journal of Nuclear Materials*, Vol. 407, pp. 119-125.

MacEwan, J.R, Lawson, V.B., 1962, "Grain Growth in Sintered Uranium Dioxide: II, Columnar Grain Growth," *Journal of the American Ceramic Society*, Vol. 45, pp. 42-46.

Mic, 2015, “Fourier Series and Square Wave Approximation,” from http://firsttimeprogrammer.blogspot.com/2015/04/fourier-series-and-square-wave.html

Michels, L. C., Poeppel R. B., Neimark, L.A., 1970, “Movement Of Fission Gas Bubbles And Inclusions In Mixed-Oxide Fuel,” Argonne National Lab., Ill..

Millett, P.C., et. al., 2011, “Phase-field simulation of irradiated metals, Part I: Pore kinetics” *Computational Materials Science*, Vol. 50, pp. 949-959.

Nabiollahi, N. et al., 2014, "Microstructure simulation of grain growth in Cu Through Silicon Via using phase-field modeling," *15th International Conference on Thermal, Mechanical and Mulit-Physics Simulation and Experiments in Microelectronics and Microsystems*.

Nichols, F.A., 1967, “Theory of columnar grain growth and central pore formation in oxide fuel rods,” *Journal of Nuclear Materials*, Vol. 22, pp. 214-222.

Nichols, F.A., 1968, “Pore migration in ceramic fuel elements,” *Journal of Nuclear Materials*, Vol. 27, pp. 137.

Nichols, F.A., 1969, “Kinetics of diffusional motion of pores in solids: A review,” *Journal of Nuclear materials*, Vol. 30, pp. 143-165.

Nichols, F.A., 1972, “On the diffusional mobilities of particles, pores and loops,” *Acta Metallurgica*, Vol. 20, pp. 207.

Nichols, F.A., 1979, “On the thermal gradient migration of lenticular pores,” *Journal of Nuclear Materials*, Vol. 84, pp. 319.

Ohse, R.W., 1964, “High-Temperature Vapor-Pressure Studies of UO2 by the Effusion Method and Its Thermodynamic Interpretation,” *Journal of Chemical Physics*, Vol. 44., pp. 1375-1377.

Olander, D.R., 1976, *Fundamental Aspects of Nuclear Reactor Fuel Elements*, Technical Information Center, Energy Research and Development Administration, Oak Ridge, TN.

Oldfield, W., Markworth, A.J., 1969, "The theory of bubble migration applied to irradiated materials," *Materials Science and Engineering*, Vol. 4.6, pp. 353-66.

Olsen, C. S., 1979, “UO2 Pore Migration and Grain Growth Kinetics,” Rep. Idaho Falls: IASMiRT.

Onsager, L., 1931, “Reciprocal Relations in Irreversible Processes. I.,” *Physical Review*, Vol. 37, pp. 405-426.

Platten, J.K., 2006, "The Soret Effect: A Review of Recent Experimental Results," *Journal of Applied Mechanics*, Vol. 73, pp. 5.

Rokkam, S., et al., 2009, “Phase field modeling of pore nucleation and growth in irradiated metals,” *Modelling and Simulation in Materials Science and Engineering*, Vol. 17.

Sens, P.F., 1972, "The Kinetics of Pore Movement in UO2 Fuel Rods," *Journal of Nuclear Materials*, Vol. 43, pp. 293-307.

Speight, M.V., 1967, “The migration of gas bubbles in material subject to a temperature gradient,” *Journal of Nuclear Materials*, Vol. 13, pp. 207.

Tikare, V., Holm, E.A., 2005, "Simulation of Grain Growth and Pore Migration in a Thermal Gradient," *Journal of the American Ceramic Society*, Vol. 81, pp. 480-84.

Williamson, G. K., Cornell, R. M., 1964, "The Behavior of Fissici Product Gases in Uranium Dioxide", *Journal of Nuclear Materials*, Vol. 13, pp. 278-280.

Zhang, L., et al., 2012, "Phase-field Modeling of Temperature Gradient Driven Pore Migration Coupling with Thermal Conduction," *Computational Materials Science* , Vol. 56, pp. 161-65.

APPENDIX

Editor - /Users/meegenrc/Desktop/Appendix/Global_Var.m

Global_Var.m | Update_CH.m | CH_Run.m

```
% ------------------------------------------------
% Define global variables for Cahn-Hilliard Eq.
% ------------------------------------------------

global c co;
global kappa;
global dt;
global M;
global nx;
global ny;
global nxy;
global k2 k4;
global KX KY;
global count2;

% ------------------------------------------------
% Initialize variables:
% ------------------------------------------------

dx = 1.0;
dy = 1.0;
nx = 512;
ny = 128;
nxy = nx*ny;
dt = 0.1;
kappa = 1.0;
M = 1.0;

%------------------------------------------------
%Define the pore position, size, and concentration
%------------------------------------------------
c = zeros(nx,ny) + 0.02;
for i = 1:nx
    for j = 1:ny
        r = ((i-480)^2 + (j-64)^2);          %initial pore center
        if r < 256                           %corresponds to pore diameter
            c(i,j) = 1.0;
        end
    end
end

kx1 = mod( 1/2 + (0:(nx-1))/nx, 1) - 1/2;
kx = kx1*(2*pi/dx);
ky1 = mod( 1/2 + (0:(ny-1))/ny, 1) - 1/2;
ky = ky1*(2*pi/dy);
[KX,KY] = meshgrid(ky,kx);

k2 = KX.*KX + KY.*KY;
k4 = k2.*k2;
```

Figure A.1. Variables and initialization
Script to initialize variables including domain size, pore position, and concentration

Editor - /Users/meegenrc/Desktop/Appendix/Update_CH.m

Global_Var.m | Update_CH.m | CH_Run.m

```
1  -    global c;
2  -    global dt;
3  -    global nx;
4  -    global nxy;
5  -    global k2 k4;
6
7        % ----------------------------------------------
8        % First, calculate chemical potential:
9        % ----------------------------------------------
10
11 -    df = 4*c.^3 - 6*c.^2 + 2*c;
12
13       % ----------------------------------------------
14       % Second, forward transform 'df' and 'c':
15       % ----------------------------------------------
16
17 -    df_FFT = fft2(df)/nxy;
18 -    c_FFT = fft2(c)/nxy;
19
20       % ----------------------------------------------
21       % Third, update 'c' in fourier space, and invert:
22       % ----------------------------------------------
23
24 -    c_FFT = (c_FFT - dt*k2.*df_FFT)./(1.0 + dt*k4);
25 -    c = ifft2(c_FFT)*nxy;
26
27       % ----------------------------------------------
28       % Forth, add convection term to CH eq:
29       % ----------------------------------------------
30
31 -    x = [1:dx:ny];
32 -    y = [1:dy:nx];
33 -    [xx,yy] = meshgrid(x,y);
34
35       % ---------------------------------------------------------------
36       % Linear equations used to represent the transport velocity fields
37       % ---------------------------------------------------------------
38 -    v = -.012*yy;                  %lenticular profile, Eq. (4.10)
39       % v = .005*yy-3.1;             %bullet profile, Eq. (4.11)
40
41       %Each equation above corresponds to a particular transport velocity.
42       %In this case, the simulation will model the migration of a pore that
43       %transforms into a lenticular shape.  Eq. (4.10) can be commented out
44       %and Eq. (4.11) can then be uncommented in order to simulate the prolate
45       %morphology and its migration.
46       %---------------------------------------------------------------
47
48
49 -    c = c - dt*(circshift(v.*c,-1) - circshift(v.*c,1))/(2*dx);
```

Figure A.2. Code to update Cahn-Hilliard model
Script to update the Cahn-Hilliard model with the concentration variable. This is also where the specified transport velocity equation is used.

Editor - /Users/meegenrc/Desktop/Appendix/CH_Run.m

Global_Var.m | Update_CH.m | CH_Run.m

```
clear; clc;

% ----------------------------------------
% Define global variables
% ----------------------------------------
Global_Var;

% ----------------------------------------
% Run the simulation:
% ----------------------------------------

nsteps = 2000;                              %number of steps to go through
Mov(1) = struct('cdata',[],'colormap',[]);
count = 0;
count2 = 0;
mock=20;                                    %step size variable

for step = 1:nsteps

%----------------------------------------
% Take step forward
%----------------------------------------
    Update_CH

% ----------------------------------------
% Plot field:
% ----------------------------------------
   if step == 1 || mod(step,20) == 0
        figure(3);
        surf(c,'EdgeColor','None');
        view(2);
        axis('equal');
        colorbar;
        caxis([0.2 1]);
        count = count + 1
        Mov(count) = getframe(gcf);
   end
%----------------------------------------
end

%----------------------------------
% Movie - uncomment to create a movie
%----------------------------------
%  v = VideoWriter('voidMig2_v*c.mp4');
%  open(v);
%  writeVideo(v,Mov);
%  close(v);
```

Figure A.3. Code to run the simulation(s)
Script to run the simulation and plot the results to visualize pore migration. This script produced the images seen in Figure 5.1 and Figure 5.2.